Johann Radon Institute for
Computational and Applied Mathematics
Austrian Academy of Sciences (ÖAW)

Critical yield numbers of rigid particles settling in Bingham fluids and Cheeger sets

I.A. Frigaard, J.A. Iglesias, G. Mercier, C. Pöschl, O. Scherzer

RICAM-Report 2016-24

Critical yield numbers of rigid particles settling in Bingham fluids and Cheeger sets

Ian A. Frigaard [a1], José A. Iglesias [b2], Gwenael Mercier [c2], Christiane Pöschl [d3], and Otmar Scherzer [e2,4]

[1]Department of Mathematics and Department of Mechanical Engineering, University of British Columbia, Vancouver, BC, Canada.
[2]Johann Radon Institute for Computational and Applied Mathematics (RICAM), Austrian Academy of Sciences, Linz, Austria.
[3]Universität Klagenfurt, Klagenfurt, Austria.
[4]Computational Science Center, University of Vienna, Vienna, Austria.

Abstract

We consider the fluid mechanical problem of identifying the critical yield number Y_c of a dense solid inclusion (particle) settling under gravity within a bounded domain of Bingham fluid, i.e. the critical ratio of yield stress to buoyancy stress that is sufficient to prevent motion. We restrict ourselves to a two-dimensional planar configuration with a single anti-plane component of velocity. Thus, both particle and fluid domains are infinite cylinders of fixed cross-section. We show that such yield numbers arise from an eigenvalue problem for a constrained total variation. We construct particular solutions to this problem by consecutively solving two Cheeger-type set optimization problems. We present a number of example geometries in which these geometric solutions can be found explicitly and discuss general features of the solutions. Finally, we consider a computational method for the eigenvalue problem, which is seen in numerical experiments to produce these geometric solutions.

1 Introduction

100 years ago Eugene Bingham [9] presented results of flow experiments through a capillary tube, measuring the flow rate and pressure drop for various materials of interest. Unlike with simple viscous fluids, he recorded a "friction constant" (a stress) that must be exceeded by the pressure drop in order for flow to occur, and thereafter postulated a linear relationship between applied pressure drop and flow rate. This empirical flow law evolved into the Bingham fluid: the

[a]frigaard@math.ubc.ca
[b]jose.iglesias@ricam.oeaw.ac.at
[c]gwenael.mercier@ricam.oeaw.ac.at
[d]christiane.poeschl@aau.at
[e]otmar.scherzer@univie.ac.at

archetypical yield stress fluid. However, it was not until the 1920's that ideas of visco-plasticity became more established [10] and other flow laws were proposed e.g. [29]. These early works were empirical and focused largely at viscometric flows. Proper tensorial descriptions, general constitutive laws and variational principles waited until Oldroyd [44] and Prager [46]. These constitutive models are now widely used in a range of applications, in both industry and nature; see [5] for an up to date review.

An essential feature of Bingham fluids flows is the occurrence of plugs: that is regions within the flow containing fluid that moves as a rigid body. This occurs when the deviatoric stress falls locally below the yield stress, which is a physical property of the fluid. Plug regions may occur either within the interior of a flow or may be attached to the wall. Generally speaking, as the applied forcing decreases, the plug regions increase in size and the velocity decreases in magnitude. It is natural that at some critical ratio of the driving stresses to the resistive yield stress of the fluid, the flow stops altogether. This critical yield ratio or *yield number*, say Y_c, is the topic of this paper.

Critical yield numbers are found for even the simplest 1D flows, such as Poiseuille flows in pipes and plane channels or uniform film flows, e.g. paint on a vertical wall. These limits have been estimated and calculated exactly for flows around isolated particles, such the sphere [8] (axisymmetric flow) and the circular disc [48, 51] (2D flow). Such flows and have practical application in industrial non-Newtonian suspensions, e.g. mined tailings transport, cuttings removal in drilling of wells, etc.

The first systematic study of critical yield numbers was carried out by Mosolov & Miasnikov [42, 43] who considered anti-plane shear flows, i.e. flows with velocity $\mathbf{u} = (0, 0, w(x_1, x_2))$ in the x_3-direction along ducts (infinite cylinders) of arbitrary cross-section Ω. These flows driven by a constant pressure gradient only admit the static solution ($w(x_1, x_2) = 0$) if the yield stress is sufficiently large. Amongst the many interesting results in [42, 43] the key contributions relate to exposing the strongly geometric nature of calculating the critical yield number Y_c. Firstly, they show that Y_c can be related to the maximal ratio of area to perimeter of subsets of Ω. Secondly, they develop an algorithmic methodology for calculating Y_c for specific symmetric Ω, e.g. rectangular ducts. This methodology is extended further by [31].

Critical yield numbers have been studied for many other flows, using analytical estimates, computational approximations and experimentation. Critical yield numbers to prevent bubble motion are considered in [20, 53]. Settling of shaped particles is considered in [33, 47]. Natural convection is studied in [34, 35]. The onset of landslides are studied in [30, 32, 28] (where the terminologies "load limit analysis" and "blocking solutions" have also been used). In [24, 25] we have studied two-fluid anti-plane shear flows, that arise in oilfield cementing.

In this paper we study critical yield numbers for two-phase anti-plane shear flows, in which a particulate solid region Ω_s settles under gravity in a surrounding Bingham fluid of smaller density. As the particle settles downwards the surrounding fluid moves upwards, with zero net flow: a so called *exchange flow*. Our objective is to derive new results that set out an analytical framework and algorithmic methodology for calculating Y_c for this class of flows.

Our analysis naturally leads to the so-called Cheeger sets, that is, minimizers of the ratio of perimeter to volume inside a given domain. In recent years, starting with [36], many of their properties have been studied, particularly regularity and uniqueness in the case of convex domains [37, 12]. These sets constitute examples of explicit solutions to the total variation flow, which has motivated their investigation [3, 6, 7].

A related line of research is the use of total variation regularization in image processing. In particular, set problems like those treated here appear in image segmentation [17] and as the problem solved by the level sets of minimizers [14, 1, 13] of the Rudin Osher Fatemi functional [50]. The analogy between anti-plane shear flows of yield stress fluids and imaging processing techniques has been exploited previously by the authors in the context of nonlinear diffusion filtering using total variation flows or bounded variation type regularization. In our previous work [23, 26] we exploited physical insights from the fluid flow problem in order to derive optimal stopping times for diffusion filtering. In this paper image processing insights are applied to the fluid flow problems.

1.1 Summary

Let us describe the key points of what follows. In all of this paper we consider geometries consisting of infinite cylinders and anti-plane velocities. First, we write the simplified Navier-Stokes equations for the inclusion of a Newtonian fluid in a Bingham fluid, and the corresponding variational formulation. Then, through the notion of Γ-convergence, we make the viscosity of the inclusion tend to infinity, that is, we study the flow of a solid inclusion into a Bingham fluid.
We recall the usual notion of critical yield number, seen as the supremum of an eigenvalue quotient (3.8) in the standard Sobolev space H^1, which writes after simplification as a minimization of total variation with constraints.
Since it is well known that such a problem does not necessarily have a solution in H^1, we relax this problem enlarging the admissible space to functions with bounded variation, which ensures the existence of a minimizer.
We then study the relaxed and show that we can construct minimizers that attain only three values and whose level-sets are solutions of simple geometrical problems closely related to the Cheeger problem (see Def. 3.10). Furthermore, we show how the geometrical properties of Cheeger sets are reflected in the structure of our three level-set minimizer, and we give several explicit examples exhibiting the influence of the geometry of the domain and the particles in that of the solution. In particular, we emphasize the role of non-uniqueness of Cheeger sets in the non uniqueness of our minimizers.
Finally, we provide a discrete formulation that can be optimized with standard algorithms used in image processing (in our case [16]), we prove its convergence to the continuous problem, and illustrate its behavior in a non-uniqueness framework.
It has to be noticed that the restriction to anti-plane flows and equal particle velocities is fundamental in all this work. The in-plane flow remains an exciting challenge.

1.2 Outline

An outline of our paper is as follows. Section 2 outlines the physical flow models considered, deriving the yield number Y. In Section 3 we develop the background theory for the exchange flow problem, defining the critical yield number Y_c and the associated minimization problem. In Section 4 we prove the existence of minimizers attaining three different values, and prove geometric properties of the level sets. The two last sections are devoted to analytic examples and numerical computations.

2 Modelling

As discussed in Section 1 we study anti-plane shear flows of particles within a Bingham fluid. Anti-plane shear flows have velocity in a single direction and the velocity depends on the 2 other coordinate directions. We assume the solid is denser than the fluid ($\hat{\rho}_f < \hat{\rho}_s$) and align the flow direction $\hat{x}_3$ with gravity. In the anti-plane shear flow context particles (solid regions) are infinite cylinders, represented as $\Omega_s \times \mathbb{R} \subseteq \mathbb{R}^3$, moving uniformly in the $\hat{x}_3$-direction. The flows are thus described in a two-dimensional region $(\hat{x}_1, \hat{x}_2) \in \Omega$. The fluid is contained in $(\Omega_f := \Omega \backslash \Omega_s) \times \mathbb{R}$, and is considered to be a Bingham fluid. The flow variables are the deviatoric stress $\hat{\tau}$, pressure $\hat{p}$ and velocity $\hat{w}$, all of which are independent of $\hat{x}_3$. Only steady flows are considered.

The fluid is characterized physically by its density, yield stress and plastic viscosity: $\hat{\rho}_f$, $\hat{\mu}_f$ and $\hat{\tau}_Y$, respectively. We adopt a fictitious domain approach to modelling the solid phase, treating it initially as a fluid and then formally taking the solid viscosity to infinity. The solid phase density and viscosity are $\hat{\rho}_s$ and $\hat{\mu}_s$. All the above parameters are assumed constant.

The incompressible Navier-Stokes equations simplify to only the $\hat{x}_3$-momentum balance. This and the constitutive laws are:

$$\hat{\operatorname{div}}\,\hat{\tau} = \begin{cases} \hat{p}_{x_3} - \hat{\rho}_f \hat{g} & \text{in } \hat{\Omega}_f\,, \\ \hat{p}_{x_3} - \hat{\rho}_s \hat{g} & \text{in } \hat{\Omega}_s\,, \end{cases} \qquad \hat{\tau} = \begin{cases} \left(\hat{\mu}_f + \frac{\hat{\tau}_Y}{|\hat{\nabla}\hat{w}|}\right) \hat{\nabla}\hat{w} & \text{in } \hat{\Omega}_f\,, \\ \hat{\mu}_s \hat{\nabla}\hat{w} & \text{in } \hat{\Omega}_s\,, \end{cases} \tag{2.1}$$

where $\hat{g}$ is the gravitational acceleration. Strictly speaking the fluid constitutive law applies only to where $|\hat{\tau}| > \hat{\tau}_Y$.

The above model and variables are dimensional, for which we have adopted the convention of using the "hat" accent, e.g. $\hat{g}$. We now make the model dimensionless by scaling. In (2.1) the driving force for the motion is the density difference, which results in a buoyancy force that scales proportional to the size of the particle. Thus, we scale lengths with $\hat{L}$:

$$\hat{L} = \sqrt{\operatorname{area}(\Omega_s)}\,, \quad \mathbf{x} = (x_1, x_2) := \frac{1}{\hat{L}}(\hat{x}_1, \hat{x}_2)\,, \quad \nabla = \hat{L}\hat{\nabla}\,, \quad \operatorname{div} = \hat{L}\,\hat{\operatorname{div}}.$$

An appropriate measure of the buoyancy stress is $(\hat{\rho}_s - \hat{\rho}_f)\hat{g}\hat{L}$, which we use to scale $\hat{\tau} = (\hat{\rho}_s - \hat{\rho}_f)\hat{g}\hat{L}\tau$. For the pressure gradient in (2.1) we subtract the hydrostatic pressure gradient from the fluid phase and scale the modified

pressure gradient with $(\hat{\rho}_s - \hat{\rho}_f)\hat{g}$, defining:

$$f = \frac{\hat{p}_z - \hat{\rho}_f \hat{g}}{(\hat{\rho}_s - \hat{\rho}_f)\hat{g}}.$$

The scaled momentum equations are:

$$\operatorname{div} \tau = \begin{cases} f & \text{in } \hat{\Omega}_{x_3}\,, \\ f-1 & \text{in } \hat{\Omega}_s\,, \end{cases} \tag{2.2}$$

For the constitutive laws, we define a velocity scale $\hat{w}_0$ by balancing the buoyancy stress with a representative viscous stress in the fluid:

$$(\hat{\rho}_s - \hat{\rho}_f)\hat{g}\hat{L} = \frac{\hat{\mu}_f \hat{w}_0}{\hat{L}}.$$

Scaled constitutive laws are:

$$\tau = \frac{1}{\varepsilon}\nabla w, \text{ in } \hat{\Omega}_s; \quad \begin{cases} \tau = \left(1 + \dfrac{Y}{|\nabla w|}\right)\nabla w & |\tau| > Y, \\ |\nabla w| = 0 & |\tau| \le Y. \end{cases} \text{ in } \hat{\Omega}_f \tag{2.3}$$

We note that there are two dimensionless parameters: ε and Y, defined as:

$$\varepsilon := \frac{\hat{\mu}_f}{\hat{\mu}_s}\,, \qquad Y := \frac{\hat{\tau}_Y}{(\hat{\rho}_s - \hat{\rho}_f)\hat{g}\hat{L}}.$$

Evidently, ε is a viscosity ratio. Soon we shall consider the solid limit $\varepsilon \to 0$, and thereafter ε plays no role in our study.

The parameter Y is called the *yield number* and is central to our study. We see that physically Y balances the yield stress and the buoyancy stress. As buoyancy is the only driving force for motion, it is intuitive that there will be no flow if Y is large enough. The smallest Y for which the motion is stopped is called the *critical yield number*, Y_c, although this will be defined rigorously later.[1]

In terms of w the momentum equation is:

$$\begin{array}{rll} \operatorname{div}\left(\left(1 + \frac{Y}{|\nabla w|}\right)\nabla w\right) & = f & \text{in } \Omega_f, \\ \operatorname{div}\left(\frac{1}{\varepsilon}\nabla w\right) & = f - 1 & \text{in } \Omega_s\,. \end{array} \tag{2.4}$$

It is assumed that Ω has finite extent and at the stationary boundary we assume the no-slip condition:

$$w \equiv 0 \text{ on } \partial\Omega\,. \tag{2.5}$$

At the interface between the two phases the shear stresses are assumed continuous, leading to the transmission condition:

$$\frac{1}{\epsilon}\nabla w \cdot \mathbf{n}_s + \left(1 + \frac{Y}{|\nabla w|}\right)\nabla w \cdot \mathbf{n}_f = 0 \quad \text{on } \partial\Omega_s. \tag{2.6}$$

[1]The yield number is sometimes referred to as the yield gravity number or yield buoyancy number. As the viscous stresses are also driven by buoyancy, an alternate interpretation would be as a ratio of yield stress to viscous stress, which is referred to as the Bingham number.

Here $\mathbf{n}_s,\ \mathbf{n}_f$ denote the outer unit-normals on $\partial\Omega_s,\ \partial\Omega_f$, and the equality has to hold in a weak sense.

We note that for given f and $\varepsilon > 0$ fixed, the solution $\hat{w}_f$ of (2.4), (2.6), (2.5) is equivalently characterized as the minimizer of the functional

$$\begin{aligned} \mathcal{F}_{\epsilon,f}(w) &:= \mathcal{G}_\epsilon(w) + f\int_\Omega w \text{ with} \\ \mathcal{G}_\epsilon(w) &:= \frac{1}{2}\int_{\Omega_f} |\nabla w|^2 + \frac{1}{2\varepsilon}\int_{\Omega_s} |\nabla w|^2 + Y\int_{\Omega_f} |\nabla w| - \int_{\Omega_s} w \end{aligned} \tag{2.7}$$

over the space $H_0^1(\Omega)$.

3 Exchange Flow Problem

Physically, as a solid particle settles in a large expanse of incompressible fluid, its downwards motion causes an equal upwards motion such that the net volumetric flux is zero. Here we wish to mimic this same scenario in the anti-plane shear flow context. Therefore, we are interested in the *exchange flow problem*, which is defined as follows.

Definition 3.1. Find the pair $(w, f) \in H_0^1(\Omega) \times L^2(\Omega)$ that satisfies:

- Equation (2.4),
- the transmission condition (2.6),
- the homogeneous boundary conditions (2.5),
- and the *exchange flow* condition

$$\int_\Omega w(x)\,dx = 0\,. \tag{3.1}$$

That is, for the exchange flow problem the pressure multiplier f is adjusted such that (3.1) is satisfied. We consider two formulations of this problem, which will be shown to be equivalent:

1. Finding a saddle point of the functional

$$\mathcal{F}_\epsilon(w, f) := \mathcal{F}_{\epsilon,f}(w) \tag{3.2}$$

on $H_0^1(\Omega) \times \mathbb{R}$, with $\mathcal{F}_{\epsilon,f}$ from (2.7). In other words, f is a Lagrange multiplier in the saddle point problem for satisfying the constraint (3.1).

2. Incorporating the constraint (3.1) as part of the domain of definition. Thus we consider minimization of the functional

$$\mathcal{G}_\epsilon^\diamond(w) := \begin{cases} \mathcal{G}_\epsilon(w) & \text{if } w \in H_\diamond^1(\Omega) := \left\{w \in H_0^1(\Omega) : \int_\Omega w = 0\right\}\,, \\ +\infty & \text{for } w \in H_0^1(\Omega)\backslash H_\diamond^1(\Omega)\,. \end{cases} \tag{3.3}$$

We show in Lemma 3.3 that a minimizer of $\mathcal{G}_\epsilon^\diamond$ exists. If $\tilde{w}$ minimizes $\mathcal{G}_\epsilon^\diamond$, then the corresponding $\tilde{f}$ is determined by evaluating the left hand side of (2.4) for $\tilde{w}$.

In the following we present some basic properties of $\mathcal{F}_\epsilon$ and $\mathcal{F}_{\epsilon,f}$, which are then used to investigate the Γ-limit for $\varepsilon \to 0+$, that describes the movement of solid particles in a fluid.

Lemma 3.2. *The functional $\mathcal{F}_\epsilon(\cdot,\cdot)$ defined in (3.2) is concave-convex in the sense of Rockafellar [49], which means that it is convex with respect to the first component w, and concave with respect to the second component.*

Lemma 3.3. *The functionals $\mathcal{F}_{\epsilon,f}(\cdot)$ and $\mathcal{G}^\diamond_\epsilon(\cdot)$ attain their minimum. If the minimizer w^* of $\mathcal{F}_{\epsilon,f}(\cdot)$ satisfies $\int_\Omega w^* = 0$, then it is also a minimizer of $\mathcal{G}^\diamond_\epsilon(\cdot)$.*

Proof. In order to prove the existence of a minimizer of $w \to \mathcal{F}_{\epsilon,f}(w)$ for f fixed, we show that the functional is coercive and lower semi-continuous:

i) *The functional $\mathcal{F}_{\epsilon,f}(w)$ is coercive with respect to w.* Note that for all $\delta > 0$ and $g \in \mathbb{R}$, and denoting by $|\Omega|$ the Lebesgue measure of Ω, it follows from Poincare's inequality that

$$\begin{aligned} g\int_\Omega w &\geqslant -\frac{1}{2\delta^2}g^2 - \frac{\delta^2}{2}\left(\int_\Omega |w|\right)^2 \\ &\geqslant -\frac{1}{2\delta^2}g^2 - \frac{\delta^2}{2}|\Omega|\int_\Omega w^2 \\ &\geqslant -\frac{1}{2\delta^2}g^2 - C\frac{\delta^2}{2}|\Omega|\int_\Omega |\nabla w|^2\,, \end{aligned} \tag{3.4}$$

and thus by putting $g = -1$ it follows

$$-\int_{\Omega_s} w \geqslant -\frac{1}{2\delta^2} - C\frac{\delta^2}{2}|\Omega|\int_\Omega |\nabla w|^2\ . \tag{3.5}$$

With $g = f$ it follows from (3.4) and (3.5) that

$$f\int_\Omega w - \int_{\Omega_s} w \geqslant -\frac{1}{2\delta^2}(f^2+1) - C\delta^2|\Omega|\int_\Omega |\nabla w|^2\ .$$

Now, choosing $\delta > 0$ such that

$$0 < C\delta^2|\Omega| < \frac{1}{2}\min\left\{1, \frac{1}{\epsilon}\right\}\,,$$

the coercivity with respect to w follows.

ii) For $\epsilon < 1$, we now have $2C|\Omega| < 1/\delta^2$ and thus we see that $\mathcal{F}_{\epsilon,f}$ is bounded from below by $-C\,(f^2+1)|\Omega|$.

iii) *The functional $\mathcal{F}_{\epsilon,f}$ is weakly lower semi-continuous:* The functional $\mathcal{F}_{\epsilon,f}$ can be rewritten as

$$\mathcal{F}_{\epsilon,f}(w) = \int_\Omega g(x, w(x), \nabla w(x))dx\,,$$

where $p \to g(s,z,p)$ is convex. This, together with the boundedness of $\mathcal{F}_{\epsilon,f}$ below, ensures (see for instance [21, Theorem 1, p 468]) that $\mathcal{F}_{\epsilon,f}(w)$ is weakly lower semi-continuous.

With this (coercivity, boundedness and weak lower semi-continuity) existence of a minimizer of $w \to \mathcal{F}_{\epsilon,f}(w)$ follows immediately (see [21, Theorem 2, p.470]).

The proof of existence of minimizer of $\mathcal{F}_\epsilon^\diamond$ requires in addition to show that $H^1_\diamond(\Omega)$ is weakly closed. Therefore note first that the set $H^1_\diamond(\Omega)$ is convex (linearity of the constrained) and closed with respect to the norm topology on $H^1_\diamond(\Omega)$. From this we can conclude that $H^1_\diamond(\Omega)$ is weakly closed, so that (see [4, Theorem 3.3.2]) the functional attains a minimium on this subset. □

Corollary 3.4. *$\mathcal{F}_\epsilon(\cdot,\cdot)$ attains a saddle-point.*

Proof. We use the results of [49], stating that for a concave-convex functional K the saddle point is the only critical point of K. For our case $K = \mathcal{F}_\epsilon$ this means that

$$(0,0) \in \partial_w \nabla_f \mathcal{F}_\epsilon(w^*, f^*)\,,$$

or in other words

$$\int_\Omega w^* = 0 \text{ and } w^* = \operatorname{argmin} \mathcal{F}_{\epsilon,f}(w, f^*)\,.$$

This, in particular, means that $w^* = \operatorname{argmin} \mathcal{G}^\diamond_\epsilon(w)$. □

3.1 Solid limit

Now we want to study the behavior of the problem when $\hat{\mu}_s \to \infty$ (so that Ω_s becomes rigid), that is $\epsilon \to 0$. We will see that it leads to minimization of the functional

$$\mathcal{G}^\diamond : H^1_0(\Omega) \to \mathbb{R} \cup \{+\infty\}\ .$$
$$w \to \begin{cases} \frac{1}{2}\int_{\Omega_f} |\nabla w|^2 + Y \int_{\Omega_f} |\nabla w| - \int_{\Omega_s} w & \text{if } w \in H^1_{\diamond,c}(\Omega) \\ +\infty & \text{else} \end{cases} \tag{3.6}$$

where we define

$$H^1_{\diamond,c}(\Omega) := \left\{ w \in H^1_0(\Omega) : \int_\Omega w = 0,\ \nabla w = 0 \text{ in } \Omega_s \right\}\ .$$

Lemma 3.5. *The functionals $\mathcal{G}^\diamond_\epsilon$ defined in (3.3) $\Gamma-$converge to $\mathcal{G}^\diamond$ in $H^1_0(\Omega)$, that is for all $w \in H^1_0(\Omega)$, and all sequences $\{\epsilon_j\}_{j\in\mathbb{N}}$ converging to 0 we have:*

i) (lim inf inequality) for every sequence $\{w_j\}_{j\in\mathbb{N}}$ converging to w in the norm topology

$$\mathcal{G}^\diamond(w) \leqslant \liminf_{j\to\infty} \mathcal{G}^\diamond_{\epsilon_j}(w_j)$$

ii) (lim sup inequality) there exists a sequence $\{w_j\}_{j\in\mathbb{N}}$ converging to w in the norm topology and

$$\mathcal{G}^\diamond(w) \geqslant \limsup_{j\to\infty} \mathcal{G}^\diamond_{\epsilon_j}(w_j)\,. \tag{3.7}$$

Proof. Let $w \in H^1_0(\Omega)$ and let $\epsilon_j \to 0+$ be a decreasing sequence with limit 0.

i) For every sequence w_j converging to w in $H^1_0(\Omega)$, we have

$$\begin{aligned}\lim_{j\to\infty}\int_\Omega |w_j| &= \int_\Omega |w|\,,\\ \lim_{j\to\infty}\int_\Omega |\nabla w_j|^2 &= \int_\Omega |\nabla w|^2\,,\\ \lim_{j\to\infty}\int_\Omega w_j &= \int_\Omega w,\\ \lim_{j\to\infty}\int_{\Omega_s} w_j &= \int_{\Omega_s} w,\end{aligned}$$

such that for all $w \in H^1_{\diamond,c}(\Omega)$

$$\begin{aligned}\mathcal{G}^\diamond(w) &= \frac{1}{2}\int_{\Omega_f}|\nabla w|^2 + Y\int_{\Omega_f}|\nabla w| - \int_{\Omega_s} w\\ &\leqslant \liminf_{j\to\infty}\left(\frac{1}{\epsilon_j}\int_{\Omega_s}|\nabla w_j|^2 + \frac{1}{2}\int_{\Omega_f}|\nabla w_j|^2 + Y\int_{\Omega_f}|\nabla w_j| - \int_{\Omega_s} w_j\right)\\ &\leqslant \liminf_{j\to\infty}\mathcal{G}^\diamond_{\epsilon_j}(w_j)\ .\end{aligned}$$

In the case where w is not constant in Ω_s, $\mathcal{F}^\diamond(w) = +\infty$ and also $\liminf_{j\to\infty}\mathcal{F}_{\epsilon_j,f}(w_j) \to \infty$ since $\lim_j \int_{\Omega_s}|\nabla w_j|^2 \neq 0$ such that $\frac{1}{\epsilon_j}\int_{\Omega_s}|\nabla w_j|^2 \to \infty$.

ii) In the case where $w \notin H^1_{\diamond,c}(\Omega)$, we have

$$\limsup \mathcal{G}^\diamond_{\epsilon_j}(w) = \infty = \mathcal{G}^\diamond(w).$$

For $w \in H^1_{\diamond,c}(\Omega)$ we have that $\int_{\Omega_s}|\nabla w|^2 = 0$. This shows that the constant sequence $w_j \equiv w$ satisfies (3.7).

□

Since the $\mathcal{G}^\diamond_\epsilon(\cdot)$ are clearly equicoercive we conclude (see [11, Theorem 1.21]) that

Corollary 3.6. *The sequence of minimizers of $\mathcal{G}^\diamond_\epsilon(\cdot)$ converges strongly in H^1 to the minimizer of $\mathcal{G}^\diamond(\cdot)$ as $\epsilon \to 0$.*

3.2 Critical yield numbers and total variation minimization

We now want to identify the limiting yield number Y such that the solution of the exchange flow problem satisfies $w \equiv 0$ in Ω, i.e. both solid and fluid motions are stagnating. The existence and uniqueness of the exchange flow problem can be seen from the considerations in Section 3.

Definition 3.7. The critical yield number is defined as follows:

$$Y_c := \sup_{H^1_{\diamond,c}(\Omega)} \frac{\int_{\Omega_s} v}{\int_\Omega |\nabla v|}\ . \tag{3.8}$$

Assume that w_c minimizes $\mathcal{G}^\diamond$, defined in (3.6). Then, by using the Euler-Lagrange equation of the functional (3.6) in weak form and inserting as test-function the minimizer w_c, we get the estimate:

$$\begin{aligned}\int_\Omega |\nabla w_c|^2 &= \int_{\Omega_f} |\nabla w_c|^2 \\ &= \int_{\Omega_s} w_c - Y \int_{\Omega_f} |\nabla w_c| \\ &\leqslant \int_{\Omega_f} |\nabla w_c| \left[\sup_{H^1_{\diamond,c}(\Omega)} \frac{\int_{\Omega_s} v}{\int_{\Omega_f} |\nabla v|} - Y \right] \\ &= (Y_c - Y) \int_{\Omega_f} |\nabla w_c| \,.\end{aligned}$$

Thus $w_c \equiv 0$ if $Y \geqslant Y_c$.

Assumption 3.8. *We are interested in computing Y_c. Even if functions in $H^1_{\diamond,c}(\Omega)$ could take different values in different connected components of Ω_s, in what follows we restrict ourselves to functions which are constant in Ω_s. This assumption covers the cases in which Ω_s is connected (Examples 5.3, 5.4, 5.6, Figure 10), when there are two connected components arranged symetrically (Example 5.7, Figure 11), or when a physical assumption can be made that the particles are linked and have the same possible velocities (Example 5.8).*

Under assumption 3.8 we set $v = 1$ in Ω_s, and therefore we need to minimize the total variation over the set

$$H^1_{\diamond,1}(\Omega) := \left\{ v \in H^1_0(\Omega) : \int_\Omega v = 0 \,,\ v \equiv 1 \text{ in } \Omega_s \right\} \,. \tag{3.9}$$

It is easy to see that this functional does not necessarily attain a minimum. Hence we use standard relaxation techniques.

Relaxation. A function $u \in L^1(\mathbb{R}^2)$ is said to be of bounded variation, when its distributional gradient Du is a (vector valued) Radon measure with finite mass, that is

$$\begin{aligned}TV(u) &:= |Du|\left(\mathbb{R}^2\right) \\ &= \sup \left\{ \int_\Omega u \ \operatorname{div} z \ dx : z \in C^\infty_0(\mathbb{R}^2;\mathbb{R}^2), |z|_{L^\infty(\mathbb{R}^2;\mathbb{R}^2)} \leqslant 1 \right\} \\ &< +\infty.\end{aligned}$$

The class of such functions is denoted by $BV(\mathbb{R}^2)$. It is a Banach space when endowed with the norm

$$\int_{\mathbb{R}^2} |u(x)| \, dx + |Du|\left(\mathbb{R}^2\right) \,.$$

We recall that $BV(\mathbb{R}^2) \subseteq L^2(\mathbb{R}^2)$.

The relaxation of minimizing TV in $H^1_{\diamond,1}(\Omega)$ with respect to strong convergence in L^1 turns out to be [4, Proposition 11.3.2] minimizing total variation over the set

$$\mathrm{BV}_{\diamond,1} := \left\{ v \in BV(\mathbb{R}^2) : \int_\Omega v = 0\,,\ v \equiv 1 \text{ in } \Omega_s, v \equiv 0 \text{ in } \mathbb{R}^2 \setminus \Omega \right\}\,. \quad (3.10)$$

Since $\mathrm{BV}_{\diamond,1} \subseteq \mathrm{BV}(\widetilde{\Omega})$ and $\mathrm{BV}(\widetilde{\Omega}) \subseteq L^1(\widetilde{\Omega})$ with compact embedding ([2, Corollary 3.49]) for every bounded $\widetilde{\Omega} \supseteq \Omega$ with $\mathrm{dist}(\partial\Omega, \partial\widetilde{\Omega}) > 0$, the condition $\int_\Omega v = 0$ and compactness in the weak-* topology of $\mathrm{BV}(\widetilde{\Omega})$ ([2, Theorem 3.23]) imply that there exists at least one minimizer of TV in $\mathrm{BV}_{\diamond,1}$.

Remark 3.9. *Note that the total variation appearing in the relaxed problem is in $\mathbb{R}^2$, meaning that jumps at the boundary of Ω are counted. Likewise, in the rest of the paper, every time we speak of total variation with Dirichlet boundary conditions on the boundary of a set A, we mean the total variation in $\mathbb{R}^2$ of functions with their values fixed on $\mathbb{R}^2 \setminus A$.*

In the sequel we will repeatedly use the relation between total variation and perimeter of sets, that we now define.

A measurable set $E \subseteq \mathbb{R}^2$ is said to be of finite perimeter in $\mathbb{R}^2$ if $1_E \in BV(\mathbb{R}^2)$. The perimeter of E is defined as $\mathrm{Per}\, E := TV(1_E)$, where 1_E is the indicatrix (or characteristic function) of the set E.

We recall that when E is a set of finite perimeter with regular boundary (for instance, Lipschitz), its perimeter $\mathrm{Per}\, E$ coincides with $\mathcal{H}^1(\partial E)$, where $\mathcal{H}^1$ is the 1-dimensional Hausdorff measure. Moreover, we denote the Lebesgue measure of E by $|E|$, so that $|E| := \int_{\mathbb{R}^2} 1_E$.

We recall the so-called *coarea formula* for $u \in BV(\mathbb{R}^2)$ compactly supported

$$TV(u) = \int_{-\infty}^{\infty} \mathrm{Per}(u > t)\,\mathrm{d}t = \int_{-\infty}^{\infty} \mathrm{Per}(u < t)\,\mathrm{d}t, \quad (3.11)$$

as well as the *layer cake formula*, valid for $u \in L^1(\mathbb{R}^2)$

$$\int_{\mathbb{R}^2} u = \int_{-\infty}^{\infty} |\{u > t\}|\,\mathrm{d}t. \quad (3.12)$$

For more properties and references on functions of bounded variation and sets of finite perimeter we refer to [2].

Particularly important for our analysis are *Cheeger sets*:

Definition 3.10. (see [45]) Let Ω_0 be a set of finite perimeter. A set E_0 minimizing the ratio

$$E \mapsto \frac{\mathrm{Per}\, E}{|E|}$$

over subsets of Ω_0, is called a *Cheeger set* of Ω_0. The quantity

$$\lambda = \frac{\mathrm{Per}\, E_0}{|E_0|}$$

is called the *Cheeger constant* of Ω_0. We recall that if $\hat{\Omega}$ is open and bounded, at least one Cheeger set exists [38, Proposition 2.5, iii)]. In addition, since being a Cheeger set is stable by union, there exists a unique maximal (with respect to $\subset$) Cheeger set.

4 Piecewise constant minimizers

We search now for simple minimizers of TV over $\mathrm{BV}_{\diamond,1}$. We prove that one can find a minimizer that attains only three values, one of them being zero.
After investigation of the particularly simple case where Ω_s is convex, we tackle the general case in four steps.

- Starting from a generic minimizer, in Proposition 4.2, we construct a (possible different) minimizer whose negative part is constant.
- Based on the minimizer with a negative constant part, we then construct a (possible different) minimizer with constant positive part (Theorem 4.3). Thus there exists a minimizer with three different values, a negative one, a positive one (which is constrained to be 1), and 0.
- We formulate the total variation minimization for three-level functions as a geometrical problem for optimizing the characteristic sets of the positive and negative value and study the curvature of the corresponding interfaces.
- Finally, we show that we can obtain these optimized characteristic sets by solving two consecutive Cheeger-type problems (Theorem 4.10).

4.1 Ω_s is convex

Proposition 4.1. *If Ω_s is convex, then the function*

$$u_0 := 1_{\Omega_s} - \alpha 1_{\Omega_-},$$

where Ω_- is a Cheeger set of $\Omega \setminus \Omega_s$ and $\alpha = \frac{|\Omega_s|}{|\Omega_-|}$, is a minimizer of TV in $BV_{\diamond,1}$.

Proof. Let u be a minimizer. We write

$$u = u^+ - u^-, \text{ with } u^+, u^- \geqslant 0.$$

Then, we have (by the coarea formula for example)

$$TV(u) = TV(u^+) + TV(u^-). \tag{4.1}$$

Firstly, note that $u \leqslant 1$: To see this note that if $|\{u > 1\}| > 0$, then the function

$$\hat{u} := u \cdot 1_{\{0<u<1\}} + 1_{\{u\geqslant 1\}} - \frac{\int u \cdot 1_{\{0<u<1\}} + 1_{\{u\geqslant 1\}}}{\int u^+} u^-.$$

satisfies $\int \hat{u} = 0$ because $\int u^- = \int u^+$, and moreover

$$\begin{aligned} TV(\hat{u}) &= TV(u \cdot 1_{\{0<u<1\}} + 1_{\{u\geqslant 1\}}) + \frac{\int u \cdot 1_{\{0<u<1\}} + 1_{\{u\geqslant 1\}}}{\int u^+} TV(u^-) \\ &< TV(u^+) + TV(u^-), \end{aligned}$$

which contradicts that u is a minimizer.

Then, let us prove that we can choose $u^+ = 1_{\Omega_s}$. Thanks to the coarea formula, we can write

$$TV(u^+) = \int_{t=0}^{1} \operatorname{Per}(u > t)\,\mathrm{d}t.$$

Since $u = 1$ on Ω_s, for every $0 < t < 1$, we have $\{u \geqslant t\} \supset \Omega_s$ which implies that $\operatorname{Per}(u > t) \geqslant \operatorname{Per}\Omega_s$ by the convexity of Ω_s (since the projection onto a convex set is a contraction). As a result, we reduce the total variation of u^+ by replacing it with 1_{Ω_s}. Replacing then u^- by ηu^- where $\eta = \frac{|\Omega_s|}{\int u^+} < 1$, we produce a competitor $\tilde{u} = 1_{\Omega_s} - \eta u^-$, which has, since u is a minimizer, the same total variation as u.

Now, notice that $\tilde{u}^-$ minimizes total variation with constraints

$$u = 0 \text{ on } (\mathbb{R}^2 \setminus \Omega) \cup \Omega_s, \quad \int \tilde{u}^- = |\Omega_s|.$$

We can link this to the Cheeger problem in $\Omega \setminus \Omega_s$. We denote

$$\lambda = \min_{E \subset (\Omega \setminus \Omega_s)} \frac{\operatorname{Per} E}{|E|}$$

and E_0 a minimizer of this ratio.

Then, one can write, observing that for $t \leqslant 0$, $\{\tilde{u} < t\} \subset (\Omega \setminus \Omega_s)$

$$\begin{aligned} TV(\tilde{u}^-) = \int_{-\infty}^{0} \operatorname{Per}(\tilde{u} < t)\,\mathrm{d}t \geqslant \lambda \int_{-\infty}^{0} |\tilde{u} < t|\,\mathrm{d}t = \lambda \int \tilde{u}^- \\ = \lambda |\Omega_s| = \frac{\operatorname{Per} E_0}{|E_0|} |\Omega_s| = TV\left(\frac{|\Omega_s|}{|E_0|} 1_{E_0}\right). \end{aligned}$$

Finally, (4.1) implies that the function

$$u_0 := 1_{\Omega_s} - \frac{|\Omega_s|}{|E_0|} 1_{E_0}$$

is a minimizer of TV which has the expected form. □

4.2 The general case

We no longer assume that Ω_s is convex.

Now, for any minimizer u on TV in $\mathrm{BV}_{\diamond,1}$, there exists a (possibly different) minimizer in which u^- is replaced by a constant function on the characteristic set of the negative part of u^-. To prove this result, we use the following proposition:

Proposition 4.2. *Let $\Theta_+ := \operatorname{Supp} u^+$. Then,*

$$u_0 := u^+ - \frac{\int u^+}{|\Omega_-|} 1_{\Omega_-}, \tag{4.2}$$

where Ω_- is a Cheeger set of $\Omega \setminus \Theta_+$, is a minimizer of TV on $BV_{\diamond,1}$. In addition, for every $t \leqslant 0$, the level-sets $\{u < t\}$ are also Cheeger sets of $\Omega \setminus \Theta_+$.

Proof. First, we notice that u^- minimizes TV with constraints $\int u^- = \int u^+$ and $u^- = 0$ on $\Theta_+ \cup (\mathbb{R}^2 \setminus \Omega)$. Let us show that u^- minimizes

$$\frac{TV(v)}{\int v}$$

among all functions supported in $\overline{\Omega \setminus \Theta_+}$. Indeed, if we have, for such a v,

$$\frac{TV(u^-)}{\int u^-} > \frac{TV(v)}{\int v},$$

then $v^- := \frac{\int u^+}{\int v} v$ satisfies $TV(v^-) = \frac{\int u^+}{\int v} TV(v) < TV(u^-)$, which is a contradiction. Then, it is well known (see, once again, [45]) that the minimizer v can be chosen as an indicatrix of a Cheeger set Ω_- of $\Omega \setminus \Theta_+$. That shows that u_0 is a minimizer.

Now, just introduce $\lambda = \frac{\operatorname{Per}\Omega_-}{|\Omega_-|}$ and use the previous computations to write

$$\begin{aligned}\lambda \int u^+ = TV(u^-) &= \int_{-\infty}^0 \operatorname{Per}(u<t)\,\mathrm{d}t = \int_{-\infty}^0 \frac{\operatorname{Per}(u<t)}{|u<t|}|u<t|\,\mathrm{d}t \\ &\geqslant \int_{-\infty}^0 \lambda |u<t|\,\mathrm{d}t = \lambda \int u^-.\end{aligned}$$

Since $\int u^+ = \int u^-$, all these inequalities are equalities and for a.e. t, we have $\frac{\operatorname{Per}(u<t)}{|u<t|} = \lambda$ and $\{u<t\}$ is therefore a Cheeger set of $\Omega \setminus \Theta_+$. □

In the following, starting from u_0, we show that there exists another minimizer of TV if we replace u_0^+ by the indicatrix of a set Ω_1.

Theorem 4.3. *There exists a minimizer of TV in $BV_{\diamond,1}$ which has the form*

$$u_c := 1_{\Omega_1} - \frac{|\Omega_1|}{|\Omega_-|} 1_{\Omega_-}, \tag{4.3}$$

where Ω_1 is a minimizer of the functional

$$\mathcal{T}(E) := \operatorname{Per}(E) + \frac{\operatorname{Per}(\Omega_-)}{|\Omega_-|}|E| \tag{4.4}$$

over Borel sets E with $\Omega_s \subset E \subset \Omega \setminus \Omega_-$. In fact, for every $0 \leqslant t < 1$, the level-sets $E_t := \{u > t\}$ of every minimizer u minimize $\mathcal{T}$.

Proof. Let u_0 be the minimizer of TV in $\mathrm{BV}_{\diamond,1}$ from (4.2). Then

$$TV(u_0) = TV(u_0^+) + TV(u_0^-) = TV(u_0^+) + \frac{\operatorname{Per}(\Omega_-)}{|\Omega_-|}\int u_0^+$$

Then from (3.11), (3.12), and (4.4) it follows:

$$\begin{aligned}TV(u_0) &= \int_0^1 \operatorname{Per}(u_0>t) + \frac{\operatorname{Per}(\Omega_-)}{|\Omega_-|}|u_0>t|\,\mathrm{d}t \\ &= \int_0^1 \mathcal{T}(u_0>t)\,\mathrm{d}t \\ &\geq \mathcal{T}(\Omega_1).\end{aligned}$$

That means, that if we replace u^+ by 1_{Ω_1}, TV is decreased and thus

$$TV(u_c) \leqslant TV(u_0) \leqslant TV(u).$$

Because u_c satisfies $\int u_c = 0$ we see from the last inequality that u_c is a minimizer of TV in $\mathrm{BV}_{\diamond,1}$. As before, since u is a minimizer, the inequalities are equalities and we infer the last statement. □

4.3 Geometrical properties of three-valued minimizers

We introduce the set

$$M := \left\{ (E_1, E_-) \subset \Omega \mid \overset{\circ}{E_1} \cap \overset{\circ}{E_-} = \emptyset,\ \Omega_s \subset E_1 \right\}.$$

and the functional

$$\mathcal{S}(E_1, E_-) = \mathrm{Per}(E_1) + \frac{|E_1|}{|E_-|}\,\mathrm{Per}(E_-).$$

In addition, for $(E_1, E_-) \in M$ we define the function

$$u_c(E_1, E_-) = 1_{E_1} - \frac{|E_1|}{|E_-|} 1_{E_-}\ .$$

Proposition 4.4. *$\mathcal{S}$ has a minimizer in M.*

Proof. Let (E_1^n, E_-^n) be a minimizing sequence for $\mathcal{S}$ in M. The conditions $\Omega_s \subset E_1$ and $E_- \subset \Omega$ ensure that $\mathrm{Per}(E_1^n) + \mathrm{Per}(E_-^n) \leqslant C$, so that standard compactness and lower semicontinuity results for sets of finite perimeter [2] imply existence of a minimizer. □

Using Theorem 4.3, we see that the connection between minimizing TV in $\mathrm{BV}_{\diamond,1}$ and minimizing $\mathcal{S}$ is as follows:

Proposition 4.5. *If the function $u_c := u_c(\Omega_1, \Omega_-)$ minimizes TV in $BV_{\diamond,1}$, then (Ω_1, Ω_-) minimizes $\mathcal{S}$ in M. Conversely, if (Ω_1, Ω_-) minimizes $\mathcal{S}$ in M, then $u_c(\Omega_1, \Omega_-)$ minimizes TV in $BV_{\diamond,1}$.*

Remark 4.6. The proposition explains why, in the following, we consider the shape optimization problem of minimizing $\mathcal{S}$ in M.
We remark that this produces minimizers of TV in $\mathrm{BV}_{\diamond,1}$ of a certain (geometric) form, which are not necessarily all of them.

In what follows, we consider small perturbations of a minimizer (Ω_1, Ω_-) of $\mathcal{S}$ in which only one of the sets is changed. This will be enough to determine the curvature of their boundaries, which we split as follows

$$\mathcal{A}_{1-} = \{x \in \Omega : x \in \partial\Omega_1, x \in \partial\Omega_-\}, \quad \mathcal{A}_{10} = \{x \in \Omega : x \in \partial\Omega_1, x \notin \partial\Omega_-\},$$
$$\mathcal{A}_{0-} = \{x \in \Omega : x \notin \partial\Omega_1, x \in \partial\Omega_-\}, \quad \mathcal{A}_{s-} = \{x \in \Omega : x \in \partial\Omega_s, x \in \partial\Omega_-\},$$
$$\mathcal{A}_{s0} = \{x \in \Omega : x \in \partial\Omega_s, x \notin \partial\Omega_-\}\ .$$

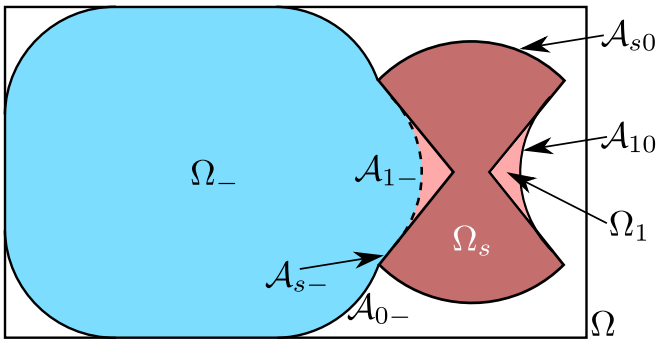

Fig. 1: Interfaces present in minimizers of $\mathcal{S}$.

We will denote by κ_1, κ_- the curvature functions of Ω_1, Ω_-, defined in $\partial\Omega_1, \partial\Omega_-$ respectively and computed using their outer normal vector n_1, n_- (i.e. a circle has positive curvature).

For a generic set of finite perimeter in $\mathbb{R}^2$ only a distributional curvature is available [40, Remark 17.7]. However, since Ω_1 and Ω_- minimize the functionals $\mathcal{S}(\cdot, \Omega_-)$ and $\mathcal{S}(\Omega_1, \cdot)$ respectively, regularity theorems for Λ-minimizers of the perimeter [40, Theorem 26.3] are applicable to them. In consequence, $\mathcal{A}_{1-}$, $\mathcal{A}_{0-}$ and $\mathcal{A}_{10} \setminus \mathcal{A}_{s0}$, are locally graphs of $C^{1,\gamma}$ functions. Combined with standard regularity theory for uniformly elliptic equations [27], one obtains higher regularity, so that, in particular, the curvatures κ_1, κ_- are defined classically on those interfaces (on $\partial\Omega_s \cap \partial\Omega_1$, no information is provided).

Proposition 4.7. *Let (Ω_+, Ω_-) be a minimizer of $\mathcal{S}$. Then, the curvatures κ_-, κ_1 of the interfaces $\mathcal{A}_{0-}$ and $\mathcal{A}_{10} \setminus \mathcal{A}_{s0}$ are given by*

$$\kappa_- = \frac{\operatorname{Per}\Omega_-}{|\Omega_-|} \text{ on } \mathcal{A}_{0-} \text{ and } \kappa_1 = -\frac{\operatorname{Per}\Omega_-}{|\Omega_-|} \text{ on } \mathcal{A}_{10} \setminus \mathcal{A}_{s0}.$$

In consequence, $\mathcal{A}_{0-}$ and $\mathcal{A}_{10} \setminus \mathcal{A}_{s0}$ are composed of pieces of circles of radius $\frac{|\Omega_-|}{\operatorname{Per}\Omega_-}$.

Proof. For every $x \in \mathcal{A}_{10} \setminus \mathcal{A}_{s0}$ we consider a perturbed domain Ω_1^w (see Figure 1), such that $\Omega_1^w = (I + \overrightarrow{w})(\Omega_1)$, where $\overrightarrow{w}$ is supported in a neighborhood of x. Calling $w := \overrightarrow{w} \cdot n_1$ and thanks to the first variation formula [40, Th. 17.5 and Rk. 17.6] we can develop the first variation of $\mathcal{S}(\cdot, \Omega_-)$ at a minimizer Ω_1 in direction w and obtain

$$\int_{\mathcal{A}_{10} \setminus \mathcal{A}_{s0}} \kappa_1 w + w \frac{\operatorname{Per}(\Omega_-)}{|\Omega_-|} \, \mathrm{d}\mathcal{H}^1 = 0.$$

Since w was arbitrary, we get the optimality condition for Ω_1:

$$\kappa_1 + \frac{\operatorname{Per}(\Omega_-)}{|\Omega_-|} = 0 \quad \text{in } \mathcal{A}_{10} \setminus \mathcal{A}_{s0}.$$

Proceeding similarly for Ω_- we obtain

$$\frac{1}{|\Omega_1|} \left(\frac{\kappa_-}{|\Omega_-|} - \frac{\operatorname{Per}(\Omega_-)}{|\Omega_-|^2} \right) = 0 \quad \text{in } \mathcal{A}_{0-}.$$

This shows that the curvatures of $\mathcal{A}_{1-} \setminus \mathcal{A}_{s-}$ and $\mathcal{A}_{1-} \setminus \mathcal{A}_{s-}$ are constant with values $\kappa_1 = -\kappa_- = \frac{\mathrm{Per}(\Omega_-)}{|\Omega_-|}$. This in particular shows that the interfaces are composed of circles of radii $\frac{|\Omega_-|}{\mathrm{Per}(\Omega_-)}$. □

Proposition 4.8. *Let (Ω_+, Ω_-) be a minimizer of $\mathcal{S}$. Then*

$$\kappa_- = \frac{\mathrm{Per}\,\Omega_-}{|\Omega_-|} = -\kappa_1 \text{ on } \mathcal{A}_{1-} \setminus \mathcal{A}_{s-}.$$

In particular, $\mathcal{A}_{1-} \setminus \mathcal{A}_{s-}$ consists of pieces of circle with the same radius as in Proposition 4.7.

Proof. First, we note that since $\mathcal{A}_{1-} \setminus \mathcal{A}_{s-} \subset \partial\Omega_1 \cap \partial\Omega_-$, we must have

$$\kappa_1 = -\kappa_- \text{ on } \mathcal{A}_{1-} \setminus \mathcal{A}_{s-}.$$

Now, we perturb Ω_1 while keeping Ω_- fixed. In this context, Ω_1 is a minimizer of $E \mapsto \mathcal{S}(E, \Omega_-)$ with constraints $E \subset \Omega$ and $\Omega_1 \cap E = \emptyset$. Since Ω_- is fixed the second constraint allows only inward perturbations. We therefore perturb Ω_1 in its exterior normal direction with a function $w \leqslant 0$ supported in $\mathcal{A}_{1-} \setminus \mathcal{A}_{s-}$. The variation formula for Ω_1 in direction w provides

$$\int_{\mathcal{A}_{1-} \setminus \mathcal{A}_{s-}} \kappa_1 w + \int w \frac{\mathrm{Per}(\Omega_-)}{|\Omega_-|}\, \mathrm{d}\mathcal{H}^1 \geqslant 0,$$

which yields

$$\kappa_1 \leqslant -\frac{\mathrm{Per}(\Omega_-)}{|\Omega_-|} \text{ on } \mathcal{A}_{1-} \setminus \mathcal{A}_{s-}.$$

Now, we fix Ω_1 and perturb Ω_- similarly with $w \leqslant 0$, again supported in $\mathcal{A}_{1-} \setminus \mathcal{A}_{s-}$ (so the perturbation goes inside Ω_-). Since Ω_- now minimizes $\mathcal{S}(\Omega_1, \cdot)$, we get

$$\int_{\mathcal{A}_{1-} \setminus \mathcal{A}_{s-}} w\kappa_- \frac{|\Omega_1|}{|\Omega_-|} - w\frac{|\Omega_1|}{|\Omega_-|^2} \mathrm{Per}(\Omega_-)\, \mathrm{d}\mathcal{H}^1 \geqslant 0,$$

which gives

$$\kappa_- \leqslant \frac{\mathrm{Per}(\Omega_-)}{|\Omega_-|} \text{ on } \mathcal{A}_{1-} \setminus \mathcal{A}_{s-}.$$

This provides the assertion. □

Proposition 4.9. *Let E be a connected component of $\Omega \setminus (\Omega_- \cup \Omega_1)$ such that $\partial E \cap \partial\Omega = \emptyset$. Then, $(\Omega_1 \cup E, \Omega_-)$ and $(\Omega_1, \Omega_- \cup E)$ both belong to M and minimize $\mathcal{S}$.*

Proof. We abbreviate $\lambda = \frac{\mathrm{Per}\,\Omega_-}{|\Omega_-|}$. Then because $E \cap \Omega_- = E \cap \Omega_1 = \emptyset$, the pairs $(\Omega_1 \cup E, \Omega_-)$ and $(\Omega_1, \Omega_- \cup E)$ both belong to M we have

$$\mathrm{Per}(\Omega_1 \cup E) + \lambda|\Omega_1 \cup E| \geqslant \mathrm{Per}(\Omega_1) + \lambda|\Omega_1|,$$

which implies because $E \cap \Omega_1 = \emptyset$

$$\lambda|E| \geqslant \mathrm{Per}(\Omega_1) - \mathrm{Per}(\Omega_1 \cup E). \tag{4.5}$$

Because Ω_- is a Cheeger set of $\Omega \setminus \Omega_1$, we have

$$\frac{\mathrm{Per}(\Omega_- \cup E)}{|\Omega_- \cup E|} \geqslant \frac{\mathrm{Per}(\Omega_-)}{|\Omega_-|}$$

which, because $E \cap \Omega_- = \emptyset$, implies

$$\mathrm{Per}(\Omega_- \cup E)|\Omega_-| \geqslant \mathrm{Per}(\Omega_-)(|\Omega_-| + |E|)\,,$$

which implies

$$\mathrm{Per}(\Omega_- \cup E) - \mathrm{Per}(\Omega_-) \geqslant \lambda|E|. \tag{4.6}$$

In summary, we have shown in (4.5) and (4.6) that

$$\mathrm{Per}(\Omega_- \cup E) - \mathrm{Per}(\Omega_-) \geqslant \lambda|E| \geqslant \mathrm{Per}(\Omega_1) - \mathrm{Per}(\Omega_1 \cup E).$$

Since $\partial E \cap \partial\Omega = \emptyset$ and $E \cap \Omega_- = E \cap \Omega_1 = \emptyset$, we know $\partial E \subset \partial\Omega_1 \cup \partial\Omega_-$. Furthermore, since Ω_- and E as well as Ω_1 and E are disjoint, there exists no common oriented boundary between E and Ω_-, Ω_1 and one can write [40, Theorem 16.3]

$$\mathrm{Per}(\Omega_- \cup E) - \mathrm{Per}(\Omega_-) = \mathrm{Per}(\Omega_1) - \mathrm{Per}(\Omega_1 \cup E)$$

which implies that all the inequalities above are equalities, and the set E can be joined to Ω_- or Ω_1 without changing the value of $\mathcal{S}$. □

In the following we show that one may obtain minimizers of $\mathcal{S}$ (and therefore minimizers of TV in $\mathrm{BV}_{\diamond,1}$ with three values) in two simpler steps:

1. Solve the Cheeger problem for $\Omega \setminus \Omega_s$. Let Ω_c be the maximal Cheeger set and $\lambda_c := \frac{\mathrm{Per}\,\Omega_c}{|\Omega_c|}$ its Cheeger constant.

2. Obtain the minimal (with respect to $\subset$) minimizer Ω_{1c} of

$$\mathrm{Per}(E) + \lambda_c|E| \text{ over } \{E : E \cap \Omega_c = \emptyset \text{ and } \Omega_s \subset E\}\,.$$

Note that minimizers of the second problem exist by an argument similar to Proposition 4.4.
Then, as we show in the following theorem, (Ω_{1c}, Ω_c) minimizes $\mathcal{S}$.

Theorem 4.10. *The pair (Ω_{1c}, Ω_c) minimizes $\mathcal{S}$.*

Proof. Let $\lambda := \frac{\mathrm{Per}\,\Omega_-}{|\Omega_-|}$ (by definition of the Cheeger set Ω_c, we have $\lambda \geqslant \lambda_c$). Let also E be the smallest (with respect to $\subset$) minimizer of

$$\hat{E} \mapsto \mathrm{Per}(\hat{E}) + \lambda|\hat{E}| \text{ subject to } \Omega_s \subset \hat{E}. \tag{4.7}$$

We want to show that $E \cap \Omega_- = \emptyset$, that is E is also a minimizer of $\mathrm{Per}(\cdot) + \lambda|\cdot|$ with respect to the constraints $E \cap \Omega_- = \emptyset$ and $\Omega_s \subset E$.

Because $E \setminus \Omega_-$ is admissible in (4.7),

$$\mathrm{Per}(E \setminus \Omega_-) + \lambda|E \setminus \Omega_-| \geqslant \mathrm{Per}(E) + \lambda|E|.$$

On the other hand, Ω_-, as a Cheeger set of $\Omega \setminus \Omega_1$, is a minimizer of

$$\hat{E} \to \mathrm{Per}(\hat{E}) - \lambda|\hat{E}| \text{ subject to } \hat{E} \cap \Omega_1 = \emptyset. \tag{4.8}$$

Then $\Omega_- \setminus E$ is a competitor for (4.8),

$$\mathrm{Per}(\Omega_- \setminus E) - \lambda|\Omega_- \setminus E| \geqslant \mathrm{Per}(\Omega_-) - \lambda|\Omega_-|.$$

Summing these two inequalities and using that (see [40, Exercise 16.5])

$$\mathrm{Per}(E \setminus \Omega_-) + \mathrm{Per}(\Omega_- \setminus E) \leqslant \mathrm{Per}(E) + \mathrm{Per}(\Omega_-),$$

we obtain

$$\lambda\left(|E \setminus \Omega_-| - |\Omega_- \setminus E|\right) \geqslant \lambda\left(|E| - |\Omega_-|\right).$$

Since this last inequality is an equality, it is also true for the two previous ones, and we can conclude that

$$\mathrm{Per}(E \setminus \Omega_-) + \lambda|E \setminus \Omega_-| = \mathrm{Per}(E) + \lambda|E|$$

which implies, since E is minimal with respect to the inclusion, that $E \cap \Omega_- = \emptyset$.

Similarly, if E_c is a minimizer of

$$\hat{E} \mapsto \mathrm{Per}\,\hat{E} + \lambda_c|\hat{E}| \text{ with constraint } \hat{\Omega}_s \subset E, \tag{4.9}$$

one can prove that $E_c \cap \Omega_c = \emptyset$.

We proved that Ω_1, Ω_{1c} minimize $\mathrm{Per}(\cdot) + \lambda\,|\cdot|\,,\ \mathrm{Per}(\cdot) + \lambda_c\,|\cdot|$ with the same constraint (containing Ω_s).

Hence, $\Omega_1 \cap \Omega_{1c}$ is admissible in (4.7) and $\Omega_1 \cup \Omega_{1c}$ is admissible for (4.9), which implies

$$\mathrm{Per}(\Omega_1 \cap \Omega_{1c}) + \lambda|\Omega_1 \cap \Omega_{1c}| \geqslant \mathrm{Per}\,\Omega_1 + \lambda|\Omega_1|,$$

$$\mathrm{Per}(\Omega_1 \cup \Omega_{1c}) + \lambda_c|\Omega_1 \cup \Omega_{1c}| \geqslant \mathrm{Per}\,\Omega_{1c} + \lambda_c|\Omega_{1c}|.$$

Summing these inequalities and recalling that [40, Lemma 12.22]

$$\mathrm{Per}(\Omega_- \cap \Omega_c) + \mathrm{Per}(\Omega_- \cup \Omega_c) \leqslant \mathrm{Per}(\Omega_-) + \mathrm{Per}(\Omega_c),$$

we obtain

$$\lambda_c|\Omega_1 \setminus \Omega_{1c}| \geqslant \lambda|\Omega_1 \setminus \Omega_{1c}|.$$

Then, if $\lambda_c < \lambda$ we obtain $\Omega_{1c} \supset \Omega_1$ and if $\lambda = \lambda_c$, all the inequalities above are equalities, which implies once again (using the minimality of Ω_1) that $\Omega_{1c} \supset \Omega_1$. Then, $\Omega_c \cap \Omega_1 = \emptyset$ hence Ω_c is also a Cheeger set of $\Omega \setminus \Omega_1$. □

Remark 4.11. *By the statements in the previous section about level sets of the generic minimizer u, we infer that the only lack of uniqueness present in the minimization of TV in $BV_{\diamond,1}$ is that of the corresponding geometric problems. More precisely, if the Cheeger set of $\Omega \setminus \Omega_s$ is unique, (which is shown in [12, Theorem 1] to be a generic situation), then the minimizer of TV in $BV_{\diamond,1}$ is unique as well. Indeed, with the same arguments as in the proof of Proposition 4.9, one sees that the minimizer of* (4.4) *is also unique, which implies by Proposition 4.2 and Theorem 4.3 that the level-sets of u are all uniquely determined.*

4.4 Behavior of Y_c as Ω grows large

Let Ω_0 be a convex set and $\Omega_s \subset \Omega_0$, both centered at the origin (again we assume that $|\Omega_s| = 1$). For $\alpha \geqslant 1$, let $\Omega = \alpha\Omega_0$, i.e. we consider the domain to be a scaled form of Ω_0. We note that $\Omega_s \subset \alpha\Omega_0$. We are interested in the limit of Y_c when $\alpha \to \infty$.

Proposition 4.12. *We have*

$$\lim_{\alpha\to\infty} Y_c(\alpha) = \frac{1}{\min\limits_{E\supset\Omega_s} \operatorname{Per} E}.$$

Proof. We recall that

$$Y_c(\alpha) = \frac{|\Omega_s|}{\inf_{M_\alpha} \mathcal{S}},$$

where

$$M_\alpha := \left\{ (E_1, E_-) \subset \alpha\Omega_0 \mid \overset{\circ}{E_1} \cap \overset{\circ}{E_-} = \emptyset,\ \Omega_s \subset E_1 \right\}.$$

Then, noticing that for every $\tilde{\Omega}$ such that $\Omega_s \subset \tilde{\Omega} \subset \alpha\Omega_0$ we have $(\tilde{\Omega}, \alpha\Omega_0 \setminus \tilde{\Omega}) \in M_\alpha$, one can write

$$\begin{aligned}
\inf_{M_\alpha} \mathcal{S} &\leqslant \mathcal{S}\left(\tilde{\Omega}, \alpha\Omega_0 \setminus \tilde{\Omega}\right) \\
&= \operatorname{Per}(\tilde{\Omega}) + \frac{\operatorname{Per}(\alpha\Omega_0) + \operatorname{Per}(\tilde{\Omega})}{|\alpha\Omega_0| - |\Omega_s|}|\tilde{\Omega}| \\
&\leqslant \operatorname{Per}(\tilde{\Omega}) + \frac{\alpha \operatorname{Per}(\Omega_0) + \operatorname{Per}(\tilde{\Omega})}{\alpha^2|\Omega_0| - 1}|\tilde{\Omega}| \xrightarrow[\alpha\to\infty]{} \operatorname{Per}(\tilde{\Omega}).
\end{aligned}$$

On the other hand, for every $(E_1, E_-) \in M_\alpha$,

$$\mathcal{S}(\tilde{\Omega}, \alpha\Omega_0 \setminus \tilde{\Omega}) \geqslant \operatorname{Per}(\tilde{\Omega}).$$

Optimizing in $\tilde{\Omega}$ establishes the result. □

Remark 4.13. *If Ω_s is indecomposable (i.e., 'connected' in an adequate sense for this framework), we have by [22, Proposition 5] that*

$$\min_{E\supset\Omega_s} \operatorname{Per} E = \operatorname{Per}(\operatorname{Co}(\Omega_s)),$$

where $\operatorname{Co}(X)$ is the convex envelope of X.

Remark 4.14. *As may be seen in examples 5.3 & 5.4, the above limit is not attained at a finite α. There is no 'critical size' at which the boundary of Ω stops playing a role. We see that the limiting Y_c is approached at least as $O(1/\alpha)$ as $\alpha \to \infty$.*

5 Application examples

In the previous section, we have seen that solutions of the eigenvalue problem may be constructed in two steps by solving two separate set optimization problems. Furthermore, the free boundaries of the optimal sets are composed of

pieces of circles of the same radius, which suggests that one might be able to use morphological operations to construct these minimizers. We introduce these now.

Definition 5.1 (Opening, Closing)**.** For a set X and $r > 0$, We define the **opening** of X with radius r by

$$Open_r(X) := \bigcup_{x:B_r(x)\subset X} B_r(x) ,$$

where $B_r(x)$ is the ball with radius r and center x (since we work in $\mathbb{R}^2$, it is a disk). Additionally we define the **closing** of X with radius r as

$$Close_r(X) := \mathbb{R}^2 \setminus \left(Open_r\left(\mathbb{R}^2 \setminus X\right)\right).$$

5.1 Morphological operations and Cheeger sets

The Cheeger problem is far from being entirely understood. Nonetheless, it is for convex sets. As a result, if Ω is convex and $\Omega_s = \emptyset$, the Cheeger set Ω_- of Ω satisfies

- Ω_- is unique,
- Ω_- is convex and $\mathcal{C}^{1,1}$,
- $\Omega_- = Open_r(\Omega)$ where r is the Cheeger constant of Ω.

In the general case, for a Cheeger set Ω_- of $\Omega \setminus \Omega_s$, only a few results are available [38]

- The boundaries of Ω_- are pieces of circles of radius $\frac{1}{\lambda}$ (λ is the Cheeger constant of $\Omega \setminus \Omega_s$) which are shorter than half the corresponding circle.
- If x_0 is a smooth point of $\partial(\Omega \setminus \Omega_s)$ and belongs to $\partial\Omega_-$, then $\partial\Omega_-$ is $\mathcal{C}^{1,1}$ around x_0 [12, Th. 2].
- We also have [38, Lemma 2.14], which basically tells that if the maximal Cheeger set of $\Omega \setminus \Omega_s$ contains a ball of radius $\frac{1}{\lambda}$, then it also contains all the balls of radius $\frac{1}{\lambda}$ obtained by rolling the first ball inside $\Omega \setminus \Omega_s$.

These properties enables us to make the following

Remark 5.2. *Let Ω and Ω_s be convex and let λ be the Cheeger constant of Ω. If $d(\Omega_s, \partial\Omega) \geqslant \frac{2}{\lambda}$, then the maximal Cheeger set of $\Omega \setminus \Omega_s$ can be obtained rolling a ball of radius $\frac{1}{\lambda_0} < \frac{1}{\lambda}$ around Ω_s ($\lambda_0 \geqslant \lambda$ being the Cheeger constant of $\Omega \setminus \Omega_s$). In particular, it fills a neighborhood of $\partial\Omega_s$ in $\Omega \setminus \Omega_s$.*

5.2 Single convex particles

We start with 2 simple examples in which a single convex particle is placed centrally within a larger convex domain.

Example 5.3. [Circular Ω]
a) Let Ω_s, Ω be two circles with radii $\frac{1}{\sqrt{\pi}}$, R, ensuring that $|\Omega_s| = 1$. Since in this case $Open_r(\Omega) = \Omega$ for all $r \leqslant R$, $\Omega_- = \Omega \setminus \Omega_s$ minimizes $S(\Omega_s, \cdot)$.

Thus, $\Omega_c = \Omega \setminus \Omega_s$ and $\Omega_{1c} = \Omega_s$. We have

$$\lambda_c = \frac{\operatorname{Per}\Omega_c}{|\Omega_c|} = \frac{2\pi R + 2\sqrt{\pi}}{\pi R^2 - 1},$$

and

$$Y_c = \frac{1}{Per(\Omega_{1c}) + \lambda_c |\Omega_{1c}|} = \frac{1}{2\sqrt{\pi} + \frac{2\pi R + 2\sqrt{\pi}}{\pi R^2 - 1}}.$$

We may also construct the minimizer of TV over $\mathrm{BV}_{\diamond,1}$, given (in cylindrical coordinates) by $v_0 : [0,\infty] \times [0,\pi] \to \mathbb{R}$:

$$v_0(r,\phi) := \begin{cases} |\Omega_s| = 1 & \text{for } 0 \leqslant r \leqslant \frac{1}{\sqrt{\pi}}, \\ -\frac{|\Omega_s|}{|\Omega| - |\Omega_s|} = -\frac{1}{R^2\pi - 1} & \text{for } \frac{1}{\sqrt{\pi}} < r \leqslant R, \\ 0 & \text{for } R < r < \infty \end{cases}$$

(evidently axisymmetric). The total variation is:

$$\begin{aligned} |Dv_0|(\Omega) &= \operatorname{Per}\Omega_s + (\operatorname{Per}\Omega_s + \operatorname{Per}\Omega) \frac{|\Omega_s|}{|\Omega| - |\Omega_s|} \\ &= 2\sqrt{\pi} + \frac{2\sqrt{\pi} + 2R\pi}{R^2\pi - 1} = \frac{1}{Y_c}. \end{aligned}$$

For $R \to \infty$ the limit is $\operatorname{Per}\Omega_s = 2\sqrt{\pi}$ and Y_c approaches $\frac{1}{2\sqrt{\pi}}$.

b) As a slight variation on the above now let Ω_s be the unit square. Again we find $\Omega_c = \Omega \setminus \Omega_s$ and $\Omega_{1c} = \Omega_s$, and hence

$$\lambda_c = \frac{\operatorname{Per}\Omega_c}{|\Omega_c|} = \frac{2\pi R + 4}{\pi R^2 - 1},$$

and

$$Y_c = \frac{1}{Per(\Omega_{1c}) + \lambda_c |\Omega_{1c}|} = \frac{1}{4 + \frac{2\pi R + 4}{\pi R^2 - 1}} \to 0.25 \text{ as } R \to \infty.$$

Example 5.4. [Square Ω]
We now consider Ω to be a square of side L. In the absence of Ω_s the optimal set Ω_- is given by $Open_{r_\infty}(\Omega)$ for $r_\infty = L/(2+\sqrt{\pi}) = 1/\lambda_c$; see [42].

a) Now consider a centrally positioned unit square Ω_s, within Ω of side $L > 1$. The optimal set Ω_- is given by $Open_r(\Omega) \setminus \Omega_s$ for some $r > 0$. We have $|Open_r(\Omega)| = |\Omega| + r^2(\pi - 4)$, $\operatorname{Per} Open_r(\Omega) = \operatorname{Per}\Omega + r(2\pi - 8)$, and to find $r = r(L)$ we use Propositions 4.7 and 4.8:

$$\frac{1}{r} = \frac{\operatorname{Per}(Open_r(\Omega) \setminus \Omega_s)}{|Open_r(\Omega) \setminus \Omega_s|} = \frac{4L + 4 + 2r(\pi - 4)}{L^2 - 1 + r^2(\pi - 4)}.$$

The resulting quadratic equation gives the optimal $r(L)$:

$$r(L) = \frac{L}{2} \frac{1 + 1/L}{1 - \pi/4} \left(1 - \sqrt{1 - (1 - \pi/4) \frac{1 - 1/L}{(1 + 1/L)}} \right).$$

We find that $r(L) < r_\infty$ with $r(L) \to r_\infty$ as $L \to \infty$ and $r(L) \to 0$ as $L \to 1^+$, as expected.

Consequently, $\Omega_c = Open_{r(L)}(\Omega) \setminus \Omega_s$ and the Cheeger constant $\lambda_c(L)$ is:

$$\lambda_c(L) = \frac{\mathrm{Per}(Open_{r(L)}(\Omega) \setminus \Omega_s)}{\left|Open_{r(L)}(\Omega) \setminus \Omega_s\right|} = \frac{4L + 4 + 2r(L)(\pi - 4)}{L^2 - 1 + r(L)^2(\pi - 4)}.$$

Again we have $\Omega_{1c} = \Omega_s$, and

$$Y_c(L) = \frac{1}{Per(\Omega_{1c}) + \lambda_c(L)|\Omega_{1c}|} = \frac{1}{4 + \lambda_c(L)}.$$

The minimizer of TV over $\mathrm{BV}_{\diamond,1}$ is constructed from the optimal sets:

$$u_{r(L)} := 1_{\Omega_s} - \frac{|\Omega_s|}{\left|Open_{r(L)}(\Omega)\right| - |\Omega_s|} 1_{Open_{r(L)}(\Omega)\setminus\Omega_s}$$

with total variation:

$$\begin{aligned}\left|Du_{r(L)}\right|(\Omega) &= \mathrm{Per}\,\Omega_s + \frac{(\mathrm{Per}\,\Omega_s + \mathrm{Per}\,\Omega + r(L)(2\pi - 8))|\Omega_s|}{|\Omega| + r(L)^2(\pi - 4) - |\Omega_s|} \\ &= 4 + \frac{(4 + 4L + r(L)(2\pi - 8))}{L^2 + r(L)^2(\pi - 4) - 1}\end{aligned}$$

b) We replace Ω_s by circle of radius $1/\sqrt{\pi}$, ensuring $|\Omega_s| = 1$, and consider $L > 2/\sqrt{\pi}$. The calculations are similar. Again the optimal set Ω_- is $Open_r(\Omega) \setminus \Omega_s$ with $r = r(L)$ determined from Propositions 4.7 and 4.8. We now find:

$$r(L) = \frac{L}{2} \frac{1 + \sqrt(\pi)/(2L)}{1 - \pi/4} \left(1 - \sqrt{1 - (1 - \pi/4)\frac{1 - 1/L^2}{(1 + \sqrt(\pi)/(2L))^2}}\right).$$

Thus, $\Omega_c = Open_{r(L)}(\Omega) \setminus \Omega_s$, $\Omega_{1c} = \Omega_s$, and

$$\lambda_c(L) = \frac{\mathrm{Per}(Open_{r(L)}(\Omega) \setminus \Omega_s)}{\left|Open_{r(L)}(\Omega) \setminus \Omega_s\right|} = \frac{4L + 2\sqrt{\pi} + 2r(L)(\pi - 4)}{L^2 - 1 + r(L)^2(\pi - 4)}.$$

$$Y_c(L) = \frac{1}{Per(\Omega_{1c}) + \lambda_c(L)|\Omega_{1c}|} = \frac{1}{2\sqrt{\pi} + \lambda_c(L)}.$$

Figure 2a plots the results of example 5.4 at different L. Interestingly, although $\lambda_c(L)$ is smaller for the circular Ω_s, it is only very marginally so. Figure 2b plots the yield limit $Y_c(L)$ for both Ω_s. Here we see a significant difference: the circular Ω_s requires a larger yield stress to prevent motion. As we have seen that $\lambda_c(L)$ is similar for both Ω_s, this difference in Y_c stems almost entirely from $Per(\Omega_{1c}) = Per(\Omega_s)$ (in these examples). We may deduce from the expressions derived that $\lambda_c(L) \sim O(1/L)$ as $L \to \infty$ and hence that $Y_c(L) \to 1/Per(\Omega_s) + O(1/L)$ as $L \to \infty$; see also Proposition 4.12. The same behaviours are observed with the earlier example 5.3, in a circle of radius R, i.e. little difference in $\lambda_c(R)$, significant difference in $Y_c(R)$, stemming primarily from $Per(\Omega_s)$, and similar asymptotic trends as $R \to \infty$.

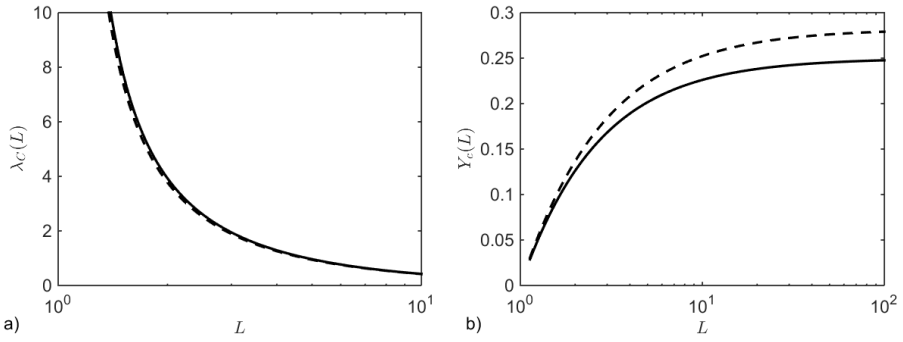

Fig. 2: Comparison of results of example 5.4 at different L: a) $\lambda_c(L)$; b) $Y_c(L)$. Circular Ω_s is marked with the broken line and square Ω_s is marked with the solid line.

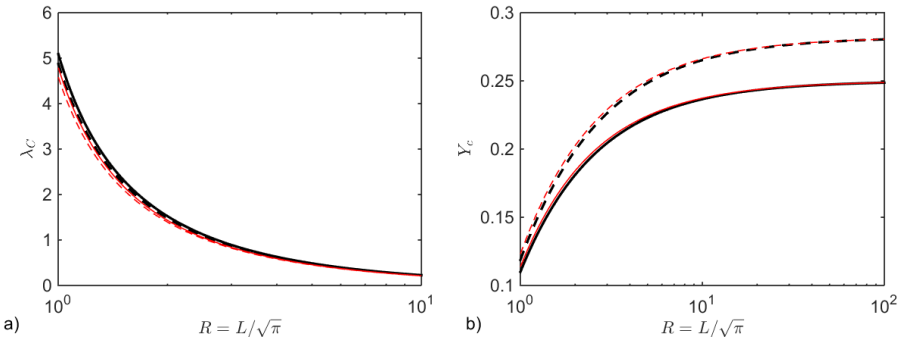

Fig. 3: Comparison of results of examples 5.3 & 5.4 at different $R = L/\sqrt{\pi}$: a) $\lambda_c(L)$; b) $Y_c(L)$. Circular Ω_s is marked with the broken line and square Ω_s is marked with the solid line. Circular Ω marked in red and square Ω in black.

We might also seek to compare examples 5.3 & 5.4 directly. The scaling introduced ensures $|\Omega_s| = 1$, matching the buoyancy force felt by each particle. By setting $L^2 = \pi R^2$ we also match the area of fluid within $\Omega \setminus \Omega_s$. Figure 3a plots $\lambda_c(R)$ and $\lambda_c(L(R))$. Figure 3b plots $Y_c(R)$ and $Y_c(L(R))$. We observe that $\lambda_c(R) < \lambda_c(L(R))$, for the same Ω_s, but again the effect is marginal and λ_c is very close for all 4 cases. Interestingly, in Figure 3b we see that by scaling $L^2 = \pi R^2$ the effects of the shape of Ω are minimized: $Y_c(R)$ and $Y_c(L(R))$ are very close for the same Ω_s, whether it be circular or square.

To summarise, these simple examples suggest that (for centrally placed convex) particles, when we have the same area of solid and the same area of fluid, the main differences in yield behaviour comes from the different perimeters of the particle. The optimal sets in $\Omega \setminus \Omega_s$ are selected such that λ_c varies primarily with the area of Ω (and less significantly with its shape). For the same size of Ω (and Ω_s) the particle with smaller perimeter has larger Y_c. An illustration of the optimal sets for the square in square case is shown in Figure 6 (left) for $L = 3.33$, for which we obtain $r = 0.600$ and $|Du_r|(\Omega) = 5.67$.

Example 5.5 (Influence of the aspect ratio and boundary)**.** We revise example

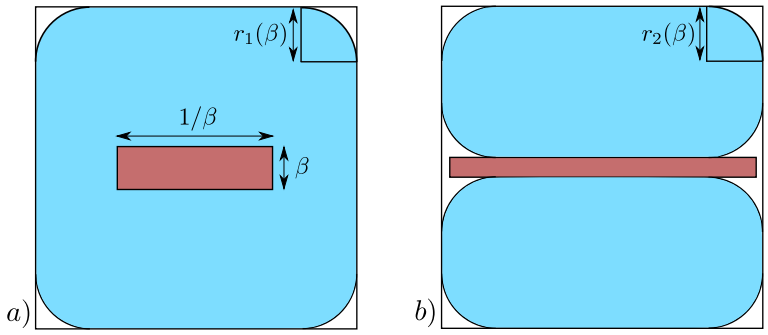

Fig. 4: Schematic of 2 different configurations for the rectangle with aspect ratio β: a) configuration 1; b) configuration 2.

5.4, keeping Ω as a square of side L and replacing Ω_s by a centrally positioned rectangle of aspect ratio β^2, i.e. the rectangle has height β and width $\beta \leq L$. Provided that β is sufficiently large there is a single Cheeger set in $\Omega \setminus \Omega_s$, given by $Open_r(\Omega) \setminus \Omega_s$ for some $r > 0$. However, for sufficiently small β:

$$\frac{1}{L} \leq \beta \leq \frac{L}{2}\left(\sqrt{1+\frac{8}{L^2}}-1\right),$$

there may be a second Cheeger set configuration, as illustrated in Figure 4.

For the first configuration we use Propositions 4.7 and 4.8 to find the radius $r_1(\beta) = 1/\lambda_{c,1}(\beta)$:

$$r_1(\beta) = \frac{L}{2}\frac{1+\frac{\beta+1/\beta}{2L}}{1-\pi/4}\left(1-\sqrt{1-(1-\pi/4)\frac{1-1/L^2}{(\frac{\beta+1/\beta}{2L})^2}}\right).$$

The second configuration gives radius $r_2(\beta) = 1/\lambda_{c,2}(\beta)$:

$$r_2(\beta) = \frac{3L-\beta}{8(1-\pi/4)}\left(1-\sqrt{1-8(1-\pi/4)\frac{L(L-\beta)}{(3L-\beta)^2}}\right).$$

It is found that for a small band of β the second configuration gives $\lambda_{c,2}(\beta) < \lambda_{c,1}(\beta)$. In both cases we have $\Omega_{1c} = \Omega_s$ and the yield limit is

$$Y_c(\beta) = \frac{1}{Per(\Omega_{1c}) + \min\{\lambda_{c,k}(\beta)\}|\Omega_{1c}|} = \frac{1}{2(\beta+1/\beta)+\min\{\lambda_{c,k}(\beta)\}}.$$

The variation of λ_c and Y_c is illustrated in Figure 5 for $L = 3$. Note that $Y_c(\beta)$ approaches the square in square results at $\beta = 1$. The difference between the two potential Y_c in Figure 5b is relatively small because for small β, $Per(\Omega_s)$ becomes relatively large.

This example also serves to demonstrate geometric non-uniqueness. In the case that $\lambda_{c,2}(\beta) < \lambda_{c,1}(\beta)$ either of the shaded regions above or below Ω_s in Figure 4b is a Cheeger set, as is the union. We may construct a minimizer of TV over $BV_{\diamond,1}$ using the characteristic functions of either set, or any linear

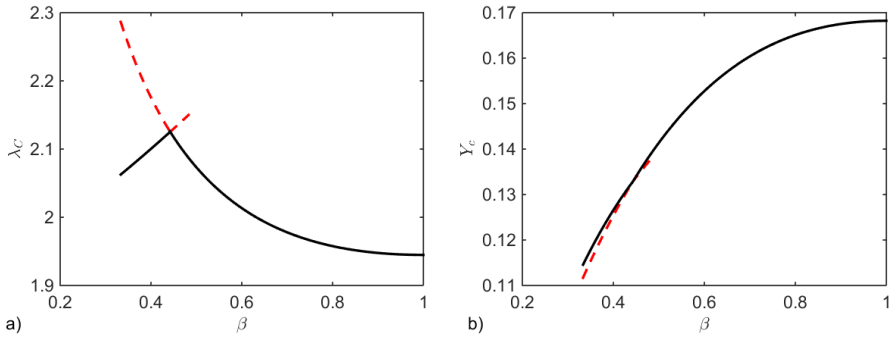

Fig. 5: Different mechanisms for the rectangle as β is varied for $L = 3$: a) $\lambda_c(\beta)$; b) $Y_c(\beta)$. The optimal values are in solid black and sub-optimal are in broken red.

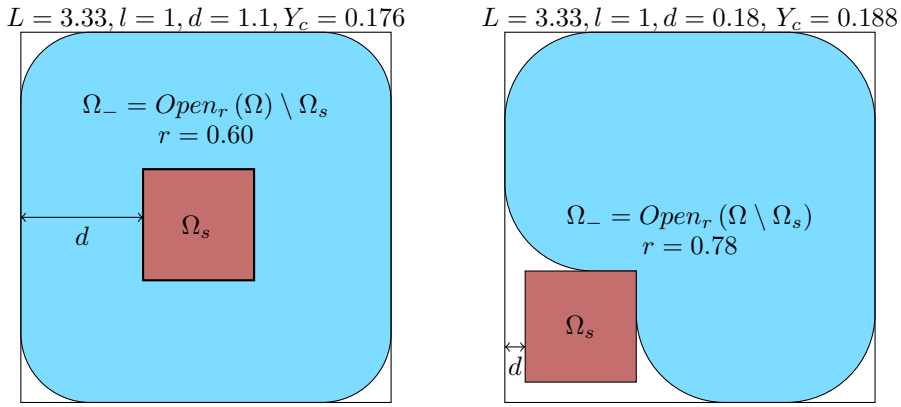

Fig. 6: In this case, area and perimeter of Ω, Ω_s are constant. We change the distance between $\partial\Omega$ and Ω_s. The critical yield number is larger if the inner set Ω_s is close to $\partial\Omega$.

combination that satisfies the condition of zero flux. As commented earlier this non-uniqueness in $\mathrm{BV}_{\diamond,1}$ stems from the geometric non-uniqueness.

Interestingly, if one were to return to the original Bingham fluid problem and approach $Y \to Y_c^-$, the velocity solution is unique and can be shown to be symmetric, i.e. the effect of viscosity here is to select a symmetric minimizer for $Y < Y_c$.

Example 5.6 (Influence of the position of Ω_s with respect to the boundary)**.** We revise example 5.4 with Ω_s again being a square with length 1. This time we move the inner square Ω_s in direction of $\partial\Omega$ and denote $d := d(\Omega_s, \partial\Omega)$. The possible minimizers have $\Omega_- = Open_r(\Omega) \setminus \Omega_s$ or $\Omega_- = Open_r(\Omega \setminus \Omega_s)$ for some r, depending on d. We illustrate this phenomenon in Figure 6.

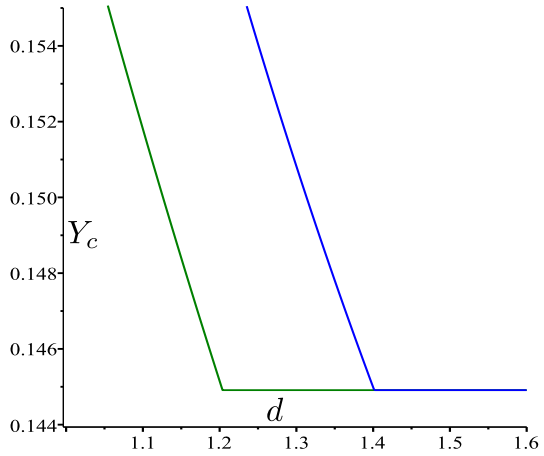

Fig. 7: Critical yield numbers in the configurations of Figure 8, with respect to the distance d between the centers of the squares. The corners in the graph represent the transition between $\Omega_- = Open_r(\Omega \setminus \Omega_s)$ and $\Omega_- = \Omega \setminus \Omega_s$.

5.3 Multiple particles

We now consider multiple particles. In the first example, we retain the fixed $|\Omega_s| = 1$ and consider the effects of increasing the number of particles. Intuitively, this increases the ratio of perimeter to area and hence we expect that Y_c will reduce, as is indeed found to be the case.

Example 5.7 (A case with nontrivial Ω_1)**.** We consider the two setups of Figure 8, where for simplicity we keep Ω circular. Figure 7 shows the dependency of the yield number with respect to the distance d between the centers of the squares. The flat regions correspond to the case where the optimal set Ω_- is equal to $\Omega \setminus \Omega_s$.

We see that the orientation has an influence on the behavior of the minimizer as well as on the critical yield number. As d is decreased below a critical value Ω_{1c} incorporates a *bridge* between the two particles. The occurrence of the bridge clearly depends on orientation of the particles, and would also vary for different shaped particles.

The phenomena of bridging between particles and of particles essentially acting independently beyond a critical distance have been studied computationally in the case of two spheres [39, 41] (axisymmetric flows) and two cylinders [52] (planar two-dimensional flows). Aside from computed examples we know of no general theoretical results related to these phenomena, e.g. what the maximal distances for bridging are.

Example 5.8 (Periodic arranged circles inside a square tube)**.** As a second example, we consider large arrays of particles, as illustrated in Figure 9, i.e. Ω is a square with length L, and Ω_s is the union of N^2 small circles with radius δ, the outermost of which are at distance a from $\partial\Omega$. Here the intention is to illustrate particle size and separation effects and therefore we emphasize that in this case $|\Omega_s|$ is not constant for different δ.

There are two types of optimal sets: For δ small (left), we have $\Omega_1 =$

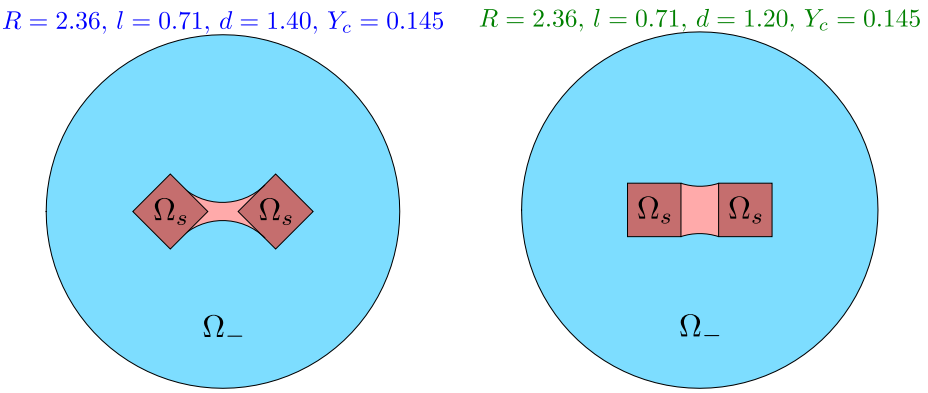

Fig. 8: Two different arrangements of squares, at the corresponding transition points. Here, the trivial and nontrivial solutions coexist and the same critical yield number appears for both orientations of the square.

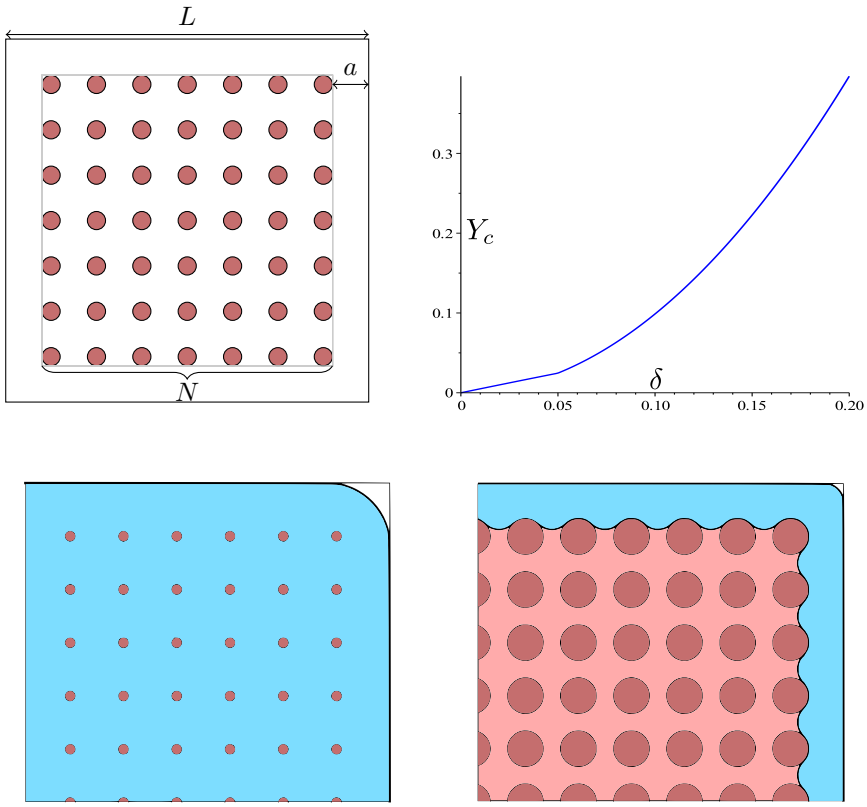

Fig. 9: Upper row, left: Setup for the periodic case. Upper row, right: Dependence of the critical yield number on δ, for $L = 12$, $N = 12$ and $a = 0.4$. The corner in the graph corresponds to the transition from trivial to bridged optimal sets. Lower row: Optimal sets for $\delta = 0.04$ and $\delta = 0.2$, when $L = 12$, $N = 12$ and $a = 0.4$.

Ω_s, $\Omega_- = Open_{\lambda^{-1}}(\Omega) \setminus \Omega_s$. For bigger δ (right), $\Omega_1 = Close_{\lambda^{-1}}(\Omega_s)$, $\Omega_- = Open_{\lambda^{-1}}(\Omega \setminus \Omega_s) = Open_{\lambda^{-1}}(\Omega) \setminus \Omega_1$ for λ the corresponding Cheeger constant. One could think of a third configuration in which isolated components of Ω_- appear between the circles of Ω_s, but it is easy to see that such a configuration has higher energy. Figure 9 (top right) shows the variation in Y_c with δ for a particular choice of parameters ($L = 12$, $N = 12$ and $a = 0.4$). The observable *kink* is where we transition between the two configurations illustrated.

Although this example is quite theoretical, this type of phenomenon occurs commonly in non-Newtonian suspension flows. In hydraulic fracturing, proppant suspensions are pumped along narrow fractures. For critical flow rates the individual dense proppant particles may act together in settling: so called *convection*, see e.g. [18]. This represents a serious risk for the process in that in *convective* settling the group of particles settles faster than when individually settling, as in the latter case secondary flows are induced on a more local scale. It is interesting that these features (local and global) are captured by the simple model here, where the yield stress fluid definitively couples the particles via bridging. Convective settling is however not in general reliant on the yield stress.

These examples also expose an interesting question concerning individual particle behaviour. Dense suspensions in shear-thinning fluids often exhibit interesting settling patterns, e.g. the column-like patterns in [19]. Such patterns are excluded in our study as we have assumed that the speed of Ω_s is uniform. There is a rich vein of interesting problems here to study. For example, if we remove the constraint of equal particle velocities, do particle arrays such as that considered above admit other optimal solutions that select patterns amongst the particles, e.g. stripes moving at different speeds, or are slight perturbations from the regular lattice favourable?

6 Numerical approach and results

There is limited knowledge available about Cheeger sets of nonconvex domains and exploring the possible configurations in explicit examples is both time consuming and relies on a certain amount of geometric intuition in defining potential configurations. Therefore, we have implemented a numerical method for the minimization of total variation in $\mathrm{BV}_{\diamond,1}$.

The algorithmic aspects are described below, but it is worth remarking that in all numerical experiments performed the method was observed to converge to an approximately piecewise constant solution (up to the unavoidable smearing of the free boundaries). Three-valued solutions have been shown to exist in the previous sections, and solutions with more levels can be easily produced in situations of non-uniqueness of Cheeger sets, as we have discussed in the context of Example 5.5. However, the existence of 'non-geometric' solutions is also not ruled out by the theory and this is another motivation for adopting a numerical approach.

6.1 Discrete saddle point formulation

The approach is to exploit the dual structure of the total variation, to apply a standard primal-dual backward-backward minimization method [16].

The problem was discretized with the upwind scheme of [15], which has the advantage of having a high degree of isotropy, and hence is helpful in correctly detecting Dirichlet boundary conditions and sharply resolving interfaces.

The constraint $\int_\Omega u = 0$ is treated through a scalar Lagrange multiplier. The boundary conditions $u \equiv 1$ on Ω_s and $u \equiv 0$ on $\mathbb{R}^2 \setminus \Omega$ are imposed by adding an indicator function term in the functional, so that the corresponding backward step is a projection. The resulting saddle-point problem is:

$$\min_{\substack{u\in X}} \max_{\substack{p\in X^4\\ q\in\mathbb{R}}} \chi_{\{1 \text{ on } D_s, 0 \text{ on } G\setminus D\}}(u) + \sum_{i,j=1}^{m,n} \left(\nabla u^{ij} \cdot p^{ij} - \chi_{\{|\cdot|_\infty \le 1\}}(p^{ij}) - q u^{ij}\right).$$

Here, $X = \mathbb{R}^{mn}$ denotes the space of real-valued discrete functions on a square grid $G = \{1, \dots, m\} \times \{1, \dots n\}$. D, D_s denote the parts of the domain corresponding to Ω, Ω_s respectively (note that to correctly account for perimeter at the boundary we must have $D \subset \{2, \dots, m-1\} \times \{2, \dots n-1\}$). The indicator function (in the convex analysis sense) of a set A is denoted by χ_A, so that $\chi_A(x) = 0$ if $x \in A$, and $+\infty$ otherwise. The expressions for ∇u^{ij} and the corresponding divergence are those of [15], which implies that each grid point (i, j) of the discrete gradient and of its multiplier $\nabla u^{ij}, p^{ij} \in \mathbb{R}^4$.

6.2 Convergence

It is well-known that finite difference discretizations of the total variation converge, in the sense of Γ-convergence with respect to the L^1 topology [15], where the discrete functionals are appropriately defined for piecewise constant functions. We now aim to demonstrate that the chosen discretization and penalization scheme correctly accounts for the boundary conditions in the limit. In this whole section, for simplicity, we assume that $n = m$ and $\Omega \Subset (0, 1)^2$. We introduce

$$R^n_{ij} := \frac{1}{n}\left(i - \frac{1}{2}, i + \frac{1}{2}\right) \times \left(j - \frac{1}{2}, j + \frac{1}{2}\right).$$

First, we need to decide which constraint to use in the discrete setting. We denote by $E - B(\frac{1}{n}) := \{x \in E, d(x, \partial E) > \frac{1}{n}\}$. Our choice is to take

$$\Omega^n_s := \bigcup_{R^n_{ij} \subset \Omega_s - B(\frac{1}{n})} R^n_{ij}$$

whereas

$$\Omega^n := [0, 1]^2 \setminus \left(\bigcup_{R^n_{ij} \subset ([0,1]^2 \setminus \Omega) - B(\frac{1}{n})} R^n_{ij} \right),$$

such that the discrete constraints are less restrictive than the continuous ones and

$$\overline{\Omega^n_s} \Subset \Omega_s, \quad \overline{[0, 1]^2 \setminus \Omega^n} \Subset [0, 1^2] \setminus \Omega. \tag{6.1}$$

We define TV^n as in [15] when the function is piecewise constant on the R^n_{ij} and $+\infty$ otherwise.

Proposition 6.1.

$$TV^n + \chi_{C^n} \xrightarrow{\Gamma - L^1} TV + \chi_C$$

where

$$C^n := \{u = 1 \text{ on } \Omega^n_s, 0 \text{ on } [0,1]^2 \setminus \Omega^n)$$

and

$$C := \{u = 1 \text{ on } \Omega_s, 0 \text{ on } [0,1]^2 \setminus \Omega)\}.$$

Proof. If $u^n \to u$ the fact that $TV(u) \leqslant \liminf TV^n(u_n)$ is standard and relies on passing to the limit in the dual formulation (see [15]) for TV^n . For χ_{C^n}, let us notice that if $\chi_C(u) = +\infty$, that is either $u \not\equiv 0$ on $[0,1]^2 \setminus \Omega$ or $u \not\equiv 1$ on Ω_s. If the latter holds, then for ε small enough, $\Omega_s \cap (\{u > 1 + 2\varepsilon\} \cup \{u < 1 - 2\varepsilon\})$ has positive measure and thanks to the L^1 convergence of u_n,

$$\Omega^n_s \cap (\{u^n > 1 + \varepsilon\} \cup \{u^n < 1 - \varepsilon\})$$

must have a positive measure for n big enough. That implies $\chi_{C^n}(u^n) = +\infty$ and the inequality is true. If $\chi_C(u) < \infty$, then $\chi_C(u) = 0$ and the inequality is also true since $C^n \subset C$.

Let now $u \in BV((0,1)^2)$. We want to construct a recovery sequence $u_n \to u$ such that $TV(u) + \chi_C(u) \geqslant \limsup TV^n(u_n) + \chi_{C^n}(u_n)$. If $u \notin C$, any $u_n \to u$ gives the inequality. If $u \in C$, then we first introduce

$$v_\delta = \rho_\delta * u$$

where ρ_δ is a convolution kernel with width δ. Then, $TV(v_\delta) \to TV(u)$ ([2, Theorem 3.9]) and, thanks to (6.1), If $\delta \leqslant \frac{1}{n}$, we have $\chi_{C^n}(v_\delta) = 0$.

We define

$$u^n_{i,j} = \fint_{R^n_{ij}} v_\delta,$$

that satisfies $\chi_{C^n}(u^n) = 0$, and compute, assuming that $u_{i+1,j} - u_{i,j} \geqslant 0$

$$\frac{u^n_{i+1,j} - u^n_{i,j}}{n} = \frac{1}{n} \fint_{R^n_{ij}} u(x + \frac{1}{n}, y) - u(x,y) \geqslant \inf_{R^n_{ij} \cup \left(R^n_{ij} + (\frac{1}{n}, 0)\right)} |\partial_x u|.$$

Then since $v_\delta \in \mathcal{C}^1$, it is clear that the right hand side converges to $|\partial_x v_\delta|$. Note that in the 'upwind' gradient of a smooth function, only one term by direction can be active, then it is also true for u^n if n is large enough and therefore $TV^n(u^n) \to TV(v_\delta)$. By a diagonal argument, we conclude. □

6.3 Examples

We present two examples of the output of numerical method. Firstly, we consider the "Pacman" shaped Ω_s within again a square Ω; see Figure 10 (left). This example induces both asymmetry (left-right) and non-convexity of Ω_s. The solution is shown in the central panel of Figure 10 and the right-hand panel shows a histogram of the solution.

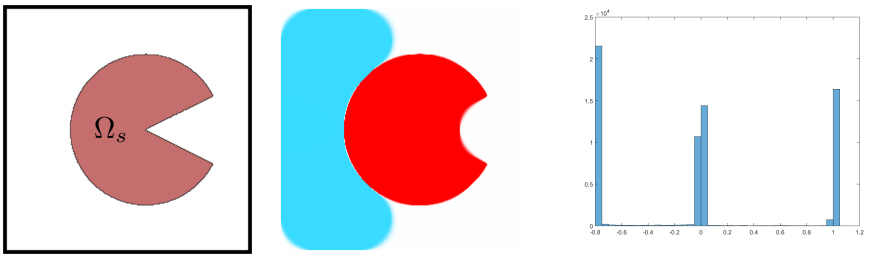

Fig. 10: Boundary conditions, result and histogram of the computed solution. In this example, one sees that the problem of minimizing S may not be reduced to a one-set problem. In this case $Y_c = 0.118$.

The second example concerns the geometry depicted in Figure 11 (top panel), in which Ω_s denotes the two L-shaped regions in the white dumbbell-shaped domain. As with the previous Example 5.5, it is apparent that there will be a Cheeger set in each half of the domain. The question is which solution the computations will converge to. Figure 11 lower, left and right) show that different minimizers are selected numerically, in this case by using different numerical resolution.

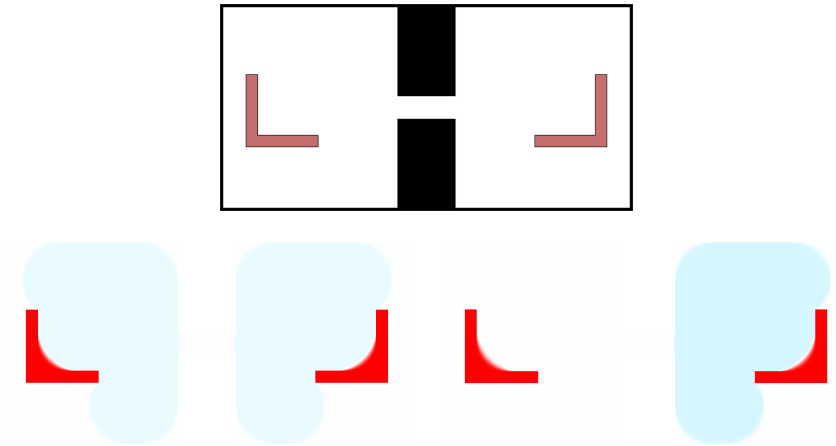

Fig. 11: Boundary conditions and results computed at two different resolutions, in a situation when uniqueness is not expected [37]. Here $Y_c = 0.087$.

Acknowledgements

This work has been supported by the Austrian Science Fund (FWF) within the national research network 'Geometry+Simulation', project S11704.

References

[1] W. K. Allard. Total variation regularization for image denoising. III. Examples. *SIAM J. Imaging Sci.*, 2(2):532–568, 2009.

[2] L. Ambrosio, N. Fusco, and D. Pallara. *Functions of bounded variation and free discontinuity problems*. Oxford Mathematical Monographs. Oxford University Press, New York, 2000.

[3] F. Andreu-Vaillo, V. Caselles, and J. M. Mazón. *Parabolic Quasilinear Equations Minimizing Linear Growth Functionals*, volume 223 of *Progress in Mathematics*. Birkhäuser Verlag, Basel, 2004.

[4] H. Attouch, G. Buttazzo, and G. Michaille. *Variational Analysis in Sobolev and BV Spaces: Applications to PDEs and Optimization.* SIAM, Society for Industrial and Applied Mathematics, 2006.

[5] N. J. Balmforth, I. A. Frigaard, and G. Ovarlez. Yielding to stress: Recent developments in viscoplastic fluid mechanics. *Ann. Rev. Fluid Mech.*, 46(1):121146, 2014.

[6] G. Bellettini, V. Caselles, and M. Novaga. The total variation flow in $\mathbb{R}^N$. *J. Differential Equations*, 184(2):475–525, 2002.

[7] G. Bellettini, V. Caselles, and M. Novaga. Explicit solutions of the eigenvalue problem $-\mathrm{div}\left(\frac{Du}{|Du|}\right) = u$ in $\mathbf{R}^2$. *SIAM J. Math. Anal.*, 36(4):1095–1129, 2005.

[8] A. N. Beris, J. A. Tsamopoulos, R. C. Armstrong, and R. A. Brown. Creeping motion of a sphere through a Bingham plastic. *J. Fluid Mech.*, 158:219–244, 1985.

[9] E. C. Bingham. An investigation of the laws of plastic flow. *Bull. Bur. Stand.*, 13:309–353, 1916.

[10] E. C. Bingham. *Fluidity and Plasticity.* McGraw-Hill, New York,, 1922.

[11] A. Braides. Γ-*convergence for beginners*, volume 22 of *Oxford Lecture Series in Mathematics and its Applications.* Oxford University Press, Oxford, 2002.

[12] V. Caselles, A. Chambolle, and M. Novaga. Some remarks on uniqueness and regularity of Cheeger sets. *Rend. Semin. Mat. Univ. Padova*, 123:191–201, 2010.

[13] V. Caselles, M. Novaga, and C. Pöschl. TV denoising of two balls in the plane. preprint, arXiv:1605.00247 [math.FA], 2016.

[14] A. Chambolle, V. Caselles, D. Cremers, M. Novaga, and T. Pock. An introduction to total variation for image analysis. In *Theoretical foundations and numerical methods for sparse recovery*, volume 9 of *Radon Ser. Comput. Appl. Math.*, pages 263–340. Walter de Gruyter, Berlin, 2010.

[15] A. Chambolle, S. E. Levine, and B. J. Lucier. An upwind finite-difference method for total variation-based image smoothing. *SIAM J. Imaging Sci.*, 4(1):277–299, 2011.

[16] A. Chambolle and T. Pock. A first-order primal-dual algorithm for convex problems with applications to imaging. *J. Math. Imaging Vision*, 40(1):120–145, 2011.

[17] T. F. Chan, S. Esedoḡlu, and M. Nikolova. Algorithms for finding global minimizers of image segmentation and denoising models. *SIAM J. Appl. Math.*, 66(5):1632–1648, 2006.

[18] M. P. Cleary and A. Fonseca. Proppant convection and encapsulation in hydraulic fracturing: Practical implications of computer and laboratory simulations. SPE paper 24825. In *67th annual technical conference and exhibition of the society of petroleum engineers, Washington, DC*, 1992.

[19] S. Daugan, L. Talini, B. Herzhaft, Y. Peysson, and C. Allain. Sedimentation of suspensions in shear-thinning fluids. *Oil and Gas Science and Technology*, 59:71–80, 2004.

[20] N. Dubash and I. A. Frigaard. Conditions for static bubbles in viscoplastic fluids. *Phys. Fluids*, 16:4319–4330, 2004.

[21] L. C. Evans. *Partial Differential Equations*, volume 19 of *Graduate Studies in Mathematics*. American Mathematical Society, Providence, RI, second edition, 2010.

[22] A. Ferriero and N. Fusco. A note on the convex hull of sets of finite perimeter in the plane. *Discrete Contin. Dyn. Syst. Ser. B*, 11(1):102–108, 2009.

[23] I. A. Frigaard, G. Ngwa, and O. Scherzer. On effective stopping time selection for visco-pastic nonlinear BV diffusion filters used in image denoising. *SIAM J. Appl. Math.*, 63:1911–1934, 2003.

[24] I. A. Frigaard and O. Scherzer. Uniaxial exchange flows of two Bingham fluids in a cylindrical duct. *IMA J. Appl. Math.*, 61:237–266, 1998.

[25] I. A. Frigaard and O. Scherzer. The effects of yield stress variation in uniaxial exchange flows of two Bingham fluids in a pipe. *SIAM J. Appl. Math.*, 60:1950–1976, 2000.

[26] I. A. Frigaard and O. Scherzer. Herschel-Bulkley diffusion filtering: non-Newtonian fluid mechanics in image processing. *Z. Angew. Math. Mech.*, 86:474–494, 2006.

[27] D. Gilbarg and N. S. Trudinger. *Elliptic partial differential equations of second order*. Classics in Mathematics. Springer-Verlag, Berlin, 2001. Reprint of the 1998 edition.

[28] R. Hassani, I. R. Ionescu, and T. Lachand-Robert. Shape optimization and supremal minimization approaches in landslides modeling. *Appl. Math. Optim.*, 52:349–364, 2005.

[29] W. H. Herschel and R. Bulkley. Konsistenzmessungen von gummi-benzollösungen. *Koll.-Z.*, 39:291–300, 1926.

[30] P. Hild, I. R. Ionescu, T. Lachand-Robert, and I. Rosca. The blocking of an inhomogeneous Bingham fluid. applications to landslides. *M2AN Math. Model. Numer. Anal.*, 36:1013–1026, 2002.

[31] R. R. Huilgol. A systematic procedure to determine the minimum pressure gradient required for the flow of viscoplastic fluids in pipes of symmetric cross-section. *J. Non-Newt. Fluid Mech.*, 136:140–146, 2006.

[32] I. R. Ionescu and T. Lachand-Robert. Generalized cheeger's sets related to landslides. *Calc. Var. Partial Differential Equations*, 23:227–249, 2005.

[33] L. Jossic and A. Magnin. Drag and stability of objects in a yield stress fluid. *AIChE J.*, 47:2666–2672, 2001.

[34] I. Karimfazli and I. A. Frigaard. Natural convection flows of a bingham fluid in a long vertical channel. *J. Non-Newt. Fluid Mech.*, 201:39–55, 2013.

[35] I. Karimfazli, I. A. Frigaard, and A. Wachs. A novel heat transfer switch using the yield stress. *J. Fluid Mech.*, 783:526–566, 2015.

[36] B. Kawohl and V. Fridman. Isoperimetric estimates for the first eigenvalue of the p-Laplace operator and the Cheeger constant. *Comment. Math. Univ. Carolin.*, 44(4):659–667, 2003.

[37] B. Kawohl and T. Lachand-Robert. Characterization of Cheeger sets for convex subsets of the plane. *Pacific J. Math.*, 225(1):103–118, 2006.

[38] G. P. Leonardi and A. Pratelli. On the Cheeger sets in strips and non-convex domains. *Calc. Var. Partial Differential Equations*, 55(1):Art. 15, 28p, 2016.

[39] B. T. Liu, S. J. Muller, and Denn M. M. Interactions of two rigid spheres translating collinearly in creeping flow in a bingham material. *J. Non-Newt. Fluid Mech.*, 113:49–67, 2003.

[40] F. Maggi. *Sets of finite perimeter and geometric variational problems*, volume 135 of *Cambridge Studies in Advanced Mathematics*. Cambridge University Press, 2012.

[41] O. Merkak, L. Jossic, and A. Magnin. Spheres and interactions between spheres moving at very low velocities in a yield stress fluid. *J. Non-Newt. Fluid Mech.*, 133:99–108, 2006.

[42] P. P. Mosolov and V. P. Miasnikov. Variational methods in the theory of the fluidity of a viscous-plastic medium. *J. Appl. Math. Mech.*, 29(3):545–577, 1965.

[43] P. P. Mosolov and V. P. Miasnikov. On stagnant flow regions of a viscous-plastic medium in pipes. *J. Appl. Math. Mech.*, 30(4):841–854, 1966.

[44] J. G. Oldroyd. A rational formulation of the equations of plastic flow for a bingham solid. *Math. Proc. Camb. Phil. Soc.*, 43:100–105, 1947.

[45] E. Parini. An introduction to the Cheeger problem. *Surv. Math. Appl.*, 6:9–21, 2011.

[46] W. Prager. *On slow visco-plastic flow.* Studies in Mathematics and Mechanics, a volume Presented to Richard von Mises by Friends, Colleagues, and Pupils. Academic Press Inc., New York, 1954.

[47] A. Putz and I. A. Frigaard. Creeping flow around particles in a Bingham fluid. *J. Non-Newt. Fluid Mech.*, 165:263–280, 2010.

[48] M. F. Randolph and G. T. Houlsby. The limiting pressure on a circular pile loaded laterally in cohesive soil. *Géotechnique*, 34:613–623, 1984.

[49] R. T. Rockafellar. Saddle-points and convex analysis. In *Differential Games and Related Topics (Proc. Internat. Summer School, Varenna, 1970)*, pages 109–127. North-Holland, Amsterdam, 1971.

[50] L. I. Rudin, S. Osher, and E. Fatemi. Nonlinear total variation based noise removal algorithms. *Phys. D*, 60(1-4):259–268, 1992. Experimental mathematics: computational issues in nonlinear science (Los Alamos, NM, 1991).

[51] D. Tokpavi, A. Magnin, and P. Jay. Very slow flow of Bingham viscoplastic fluid around a circular cylinder. *J. Non-Newt. Fluid Mech.*, 154:65–76, 2008.

[52] D. L. Tokpavi, P. Jay, and A. Magnin. Interaction between two circular cylinders in slow flow of bingham viscoplastic fluid. *J. Non-Newt. Fluid Mech.*, 157:175–187, 2009.

[53] J. Tsamopoulos, Y. Dimakopoulos, N. Chatzidai, G. Karapetsas, and M. Pavlidis. Steady bubble rise and deformation in Newtonian and viscoplastic fluids and conditions for bubble entrapment. *J. Fluid Mech.*, 601:123–164, 2008.